Design of a Small Diameter Fibre Optical Probe for Interstitial Chromophore Concentration Measurements

Master's Thesis
by
Sofia Lindgren and Pelle Ohlsson

Lund Reports on Atomic Physics, LRAP-372
Lund, January 2007

Abstract

In medical research it is often interesting to measure tissue concentration of different chromophores, such as haemoglobin or a drug. One approach is to use absorption spectroscopy. However, tissue scatters light to a large extent, varying from patient to patient, which complicates such measurements. In this report we suggest a design for an interstitial probe for measurement of absorption independent of scattering. The probe consists of two optical fibres fitted inside a needle, where the tip of the detection fibre is pulled back a certain distance compared to the tip of the source fibre. This design was evaluated using both Monte Carlo simulations and measurements in a tissue phantom. The trade off between good sensitivity to absorption and minimal influence of scattering led to an optimal pull back distance between the source fibre and detection fibre of 2 mm.

Populärvetenskaplig sammanfattning

Bland de svenskar som drabbas av cancer är prostatacancer den vanligaste diagnosen. Denna form utgör mer än en tredjedel av cancerfallen hos män. Fotodynamisk terapi är en lovande behandlingsmetod, som utvecklas av forskare bland annat vid atomfysikavdelningen på LTH. Vid denna behandling ger man patienten ett läkemedel som ansamlas i tumörcellerna. Detta är inte giftigt i sig, men aktiveras när man belyser det med ljus av rätt färg. Ett skadligt ämne bildas då som dödar tumörcellerna.

Vid behandlingen behöver man mäta bland annat koncentrationen av läkemedlet i kroppen. Målet med vårt arbete har varit att ta fram en nål för detta ändamål. I den en millimeter breda nålen finns två optiska fibrer som leder ljus in i och ut ur kroppen. Vi mäter sedan hur mycket av det inskickade ljuset som absorberats av läkemedlet innan det träffar den andra optiska fibern och leds ut ur kroppen. En bild på hur nålen med de optiska fibrerna ser ut finns i figur 1.

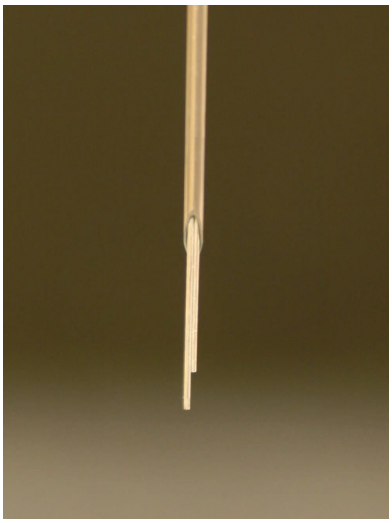

Figur 1: Bilden visar nålen och de två optiska fibrerna som sticker ut. Den ena fibern leder in ljus i kroppen medan den andra leder ut ljus. De två optiska fibrerna är 0,4 millimeter i diameter vardera.

Ett problem vid mätningar som den här är att ljus inte går rakt fram genom kroppen, utan studsar fram och tillbaka många gånger och sprids i olika riktningar. Detta gör att man inte vet hur lång väg ljuset har gått, vilket man behöver veta om man ska mäta koncentration av ett ämne. Därför vill vi utforma nålen så att ljuset alltid går lika långt, oavsett hur mycket vävnaden sprider ljuset.

För att hitta den bästa utformningen av nålen har vi gjort både datorsimuleringar och mätningar. För simuleringarna använde vi ett program som heter ASAP, där vi gjorde en modell av prostatan och de optiska fibrerna. Sedan skickade vi ljus genom modellen och mätte hur mycket ljus som gick från den ena fibern till den andra och hur lång sträcka det ljuset hade gått. Detta gjorde vi för olika värden på absorption och spridning och med fibrerna i olika positioner. Väglängden ljuset gick var i storleksordningen en centimeter. En bild av modellen finns i figur 2.

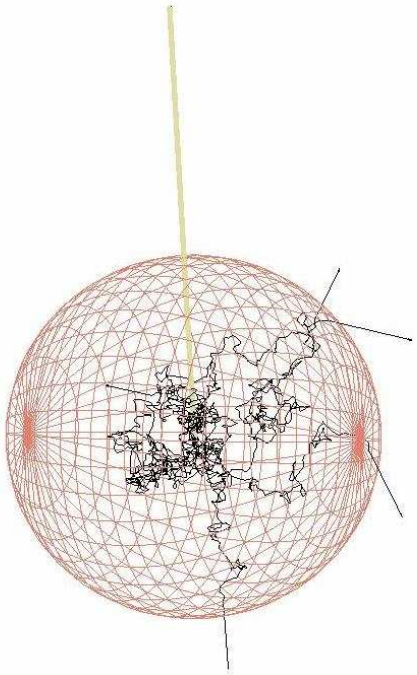

Figur 2: Bilden visar modellen som används i datorsimuleringarna. Den röda sfären är prostatan och de två instuckna optiska fibrerna syns i gult. De svarta linjerna är exempel på hur ljuset studsar runt (sprids) i vävnaden.

Vid mätningarna använde vi ett instrument som både skickade ut ljus genom den ena fibern och analyserade ljuset som skickades tillbaka i den andra fibern. Fibrerna leddes genom en nål ned i en vätska med egenskaper som liknar vävnad, en så kallad vävnadsfantom. När man använder en vävnadsfantom istället för riktig vävnad kan man lättare kontrollera hur ljuset påverkas. Vi undersökte sedan hur exakt vi kunde mäta upp koncentrationen i provet med fibrerna placerade på olika sätt i nålen. Mätuppställningen visas i figur 3.

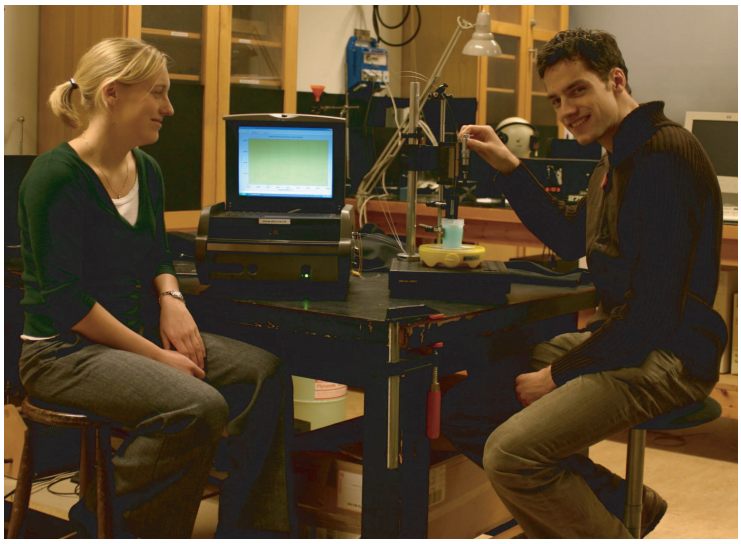

Figur 3: Rapportförfattarna i full gång med mätningarna. Mitt i bilden kan man se mätinstrumentet (lite till vänster) och bägaren med vävnadsfantomen (lite till höger).

Enligt simuleringarna och mätningarna ska avståndet mellan de två fiberspetsarna vara så litet som möjligt för att man ska kunna mäta koncentrationen utan att påverkas av hur mycket vävnaden sprider ljuset. Samtidigt vill vi att avståndet ska vara så stort som möjligt för att kunna mäta små koncentrationer. Detta tillsammans ger ett optimalt avstånd mellan fiberspetsarna på två millimeter när man mäter läkemedelskoncentration i prostatavävnad.

Contents

Chapter 1

Introduction

1.1 Background

The ability to measure the concentrations of various tissue chromophores and drugs in living tissue by the means of optical methods provides advantages in many different applications in medicine. One area where the benefits of such *in vivo* measurements are numerous is photodynamic therapy (PDT). PDT is a cancer treatment modality where a photosensitizer is administered to the patient. The photosensitizer will accumulate to a higher degree in tumour tissue than in healthy tissue and after a certain amount of time, allowing the sensitizer to build up, the tumour area is illuminated. Light is then be absorbed by the sensitizer and a chemical reaction is induced, resulting in the formation of oxidative species. The thus produced radicals cause the tissue to become necrotic.[1] However, for the treatment to be efficient, the proper light dosage should be delivered. This requires knowledge of both the optical properties of the tissue and the sensitizer concentration in the tissue to be treated. Both the intrinsic tissue absorption and the drug uptake vary between different patients and within patients, therefore it is important to have a measurement method that can be used *in vivo* to give individual information.[2]

One example of an instrument developed for this purpose is described by Mourant et al.[2,3] It consists of a white light source, a spectrometer, a computer and a fibre probe constructed for surface measurements. The fibre probe consists of one source and one detector fibre separated by a distance of 2 mm, chosen so that the absorption can be measured with minimal dependence on the scattering level within the tissue. This gives a more accurate prediction of the drug or chromophore concentration. However, due to the large diameter, this probe can only be used superficially, on e.g. skin tumours, and is not suitable for interstitial photodynamic therapy (IPDT) .

1.2 Goal

The aim of this work was to develop a fibre probe for absorption measurements to be used during interstitial photodynamic therapy (IPDT) treatment of the prostate. The probe should be designed to fit inside a needle, since the treatment is performed using brachytherapy needles. Furthermore, the probe should be used together with the already existing instrument mentioned above and it should be able to measure absorption independent of scattering. To fulfill the criterion of a small probe diameter, the fibres can not be separated, instead the tip of the detector fibre is pulled back a certain distance from the tip of the source fibre. Finding the optimal pull back distance (the "magic distance"), for which the absorption coefficient can be measured with minimal dependence on the scattering coefficient, was the main goal of this project.

1.3 Outline

The thesis starts in Chapter 2 with the theory of light propagation in tissue including a description of the transport equation, a discussion on optical properties and the Beer Lambert law. Furthermore, the theory includes fluorescence, fibre optics and different methods to measure optical properties, especially absorption. A general theory of Monte Carlo simulation is also given. In Chapter 3, the simulation program used and the experimental set-up is described. The results are given in Chapter 4 and they are discussed in Chapter 5, which also contains suggestions for further investigations. Finally, a conclusion together with a final suggestion for the probe design is made in Chapter 6. Some detailed calculations and simulation code are found in Appendices A and B.

Chapter 2

Theory

2.1 Light Propagation in Tissue

A clear medium is a medium where the refractive index is constant on a spatial scale ranging from microscopic to macroscopic, which means that the light passes straight through the material without being scattered. If, on the other hand, there are spatial variations in tissue density or dielectric constant and thus in refractive index, this will lead to scattering of the light. As the photon propagates through a scattering material like tissue, it will undergo multiple scattering as well as being absorbed.

There are two different ways of describing light propagation, based on two different physical theories: wave theory and transport theory. The electromagnetic wave theory is based on solutions of the Maxwell's equations, where the optical properties are described by the complex dielectric constant. However, in complex macroscopic problems like light propagation in tissue it is not possible to solve the wave equation and to handle the variation of the dielectric constant on a microscopic level. For this kind of problems the transport theory of radiative transfer is a better alternative.[4]

2.1.1 Transport Equation

In transport theory, light propagation is modelled by the transport equation, which is an equation of energy conservation describing the transfer of energy through a turbid medium.[4] It is a theory based on a statistical approximation of photon transport in a multiple scattering medium. The interactions between photons and tissue are described in terms of a scattering coefficient, an absorption coefficient and a scattering phase function which relates to the probability of scattering in different directions.[5]

The different contributions to the transport equation is shown schematically in Figure 2.1. The equation describes the change in radiance, $L(\mathbf{r}, \mathbf{s}, t)$ $[W/m^2 sr]$,

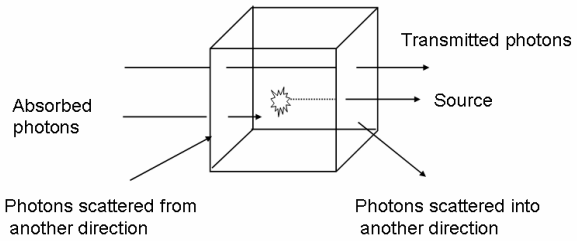

Figure 2.1: Schematic picture of the different parts of the transport equation.

i.e. the light intensity per unit solid angle, in the direction $\mathbf{s}$ inside a small volume element dV:

$$\frac{1}{c}\frac{\partial L(\mathbf{r},\mathbf{s},t)}{\partial t} = \underbrace{-\mathbf{s}\cdot\nabla L(\mathbf{r},\mathbf{s},t)}_{1} - \underbrace{\mu_a L(\mathbf{r},\mathbf{s},t)}_{2} - \underbrace{\mu_s L(\mathbf{r},\mathbf{s},t)}_{3} + \underbrace{+\mu_s \int_{4\pi} L(\mathbf{r},\mathbf{s}',t)p(\mathbf{s},\mathbf{s}')dw'}_{4} + \underbrace{q(\mathbf{r},\mathbf{s},t)}_{5} \tag{2.1}$$

The five different parts of the equation are:

1. Transmitted light, i.e. losses over the boundary dV
2. Losses due to absorbed light
3. Losses due to scattering
4. Gains due to light scattered into direction $\mathbf{s}$
5. Gains due to sources within the volume

The designations used are c $[m/s]$, the speed of light in the medium, μ_a $[m^{-1}]$, the absorption coefficient, μ_s $[m^{-1}]$, the scattering coefficient and $p(\mathbf{s},\mathbf{s}')$, the scattering phase function that gives the probability of scattering from direction $\mathbf{s}'$ into direction $\mathbf{s}$ and dw' is an infinitesimal solid angle in the direction $\mathbf{s}$. q $[W/m^3sr]$ represents the source term.[4,6]

2.1.2 Optical Properties

Absorption

When the energy of a photon matches the energy difference between two energy levels in an atom or molecule the photon can be absorbed. The energy will then be transferred to the atom or molecule, transferring it to an excited state. In tissue optics the absorption is quantified by the absorption coefficient μ_a $[m^{-1}]$,

which is defined as the probability for a photon to be absorbed per unit length. Thus, the probability of absorption in an infinitesimal distance ds is $\mu_a ds$. The mean free path for an absorption event, i.e. the mean distance a photon travels before it is absorbed, is $1/\mu_a$.[5]

Absorbing components in tissue are called chromophores. In the visible and NIR regions the most important chromophores are hemoglobin (oxygen transporting molecules found in red blood cells), water, lipids and melanin (small pigment granules in the skin, hair and eye).[4,5] In the UV wavelength range the primary absorbers are protein and amino acids and for IR wavelengths water is the most important absorber.[5] The region between approximately 630 and 1300 nm is sometimes referred to as the tissue optical window, due to the low overall absorption in this region.[1] Also, the scattering is lower for these wavelengths compared with the UV and visible wavelenghts. This means that the light in this wavelength region penetrates deeper into the tissue.[4] Absorption spectra of tissue chromophores can be seen in Figure 2.2, where the tissue optical window is indicated as well.

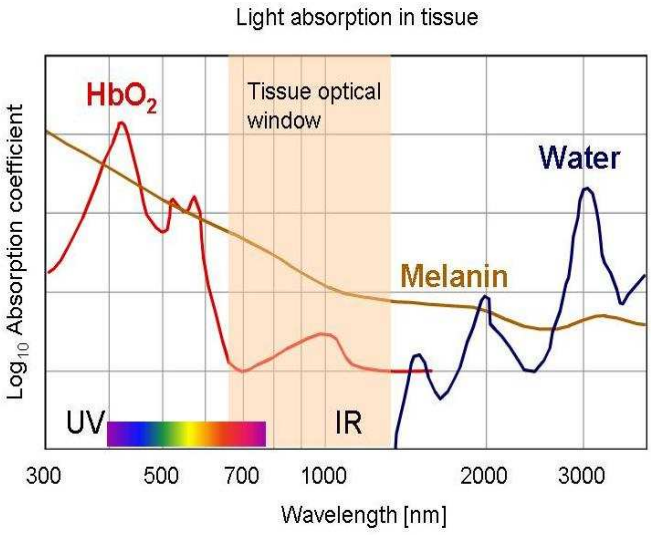

Figure 2.2: Absorption spectra of tissue chromophores adapted from Boulnois.[7] The tissue optical window is also indicated.

Reflection

When light is incident on an interface between two media with different refractive indices some of the light will be reflected. This reflection is strongly dependent on the incident angle, the polarization and the shape and structure

of the medium. However, in tissue optics the polarization of the light can often be neglected as the light sources used are often unpolarized, un exception is if the light source is a laser and the light is delivered to the tissue without the use of optical fibres. In this case the reflected intensity is governed by the resnel equations and is[1]

$$R = \frac{1}{2}\left[\frac{\sin^2(\theta_i - \theta_t)}{\sin^2(\theta_i + \theta_t)} + \frac{\tan^2(\theta_i - \theta_t)}{\tan^2(\theta_i + \theta_t)}\right]. \tag{2.2}$$

where θ_i is the angle of incidence and θ_t is the angle of transmission in the second medium. The transmission angle can be calculated from Snell's law of refraction[8]

$$n_1 \sin\theta_i = n_2 \sin\theta_t, \tag{2.3}$$

which is illustrated in Figure 2.3. In tissue a typical value for the refractive index is 1.4.[5]

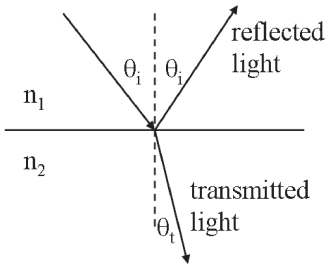

Figure 2.3: A schematic picture of the reflected and transmitted light at the boundary between two different media.

Scattering

As mentioned above, spatial variations in refractive index will lead to multiple scattering of the light. The scattering coefficient, μ_s, is defined similarly to the absorption coefficient as the probability per unit length for a photon to be scattered. The probability of scattering in an infinitesimal distance ds is then $\mu_s ds$ and the mean free path for a scattering event is $1/\mu_s$.[5]

There are mainly two ways to theoretically model high scattering: Rayleigh and Mie theory. The Rayleigh model is valid if the light is scattered by particles much smaller than the wavelength of the light. In this case, the scattered intensity follows a $1/\lambda^4$ dependence and it is isotropically distributed. For spherical scatterers of the same size as the wavelength, Mie theory, which is deduced from Maxwell's equations, is used. The intensity of the scattered light is then depending on the wavelength and the size of the scatterers, and is highly forward directed. Because of the complexity of this model, the equations are only possible to solve for a few simple geometries.[1,9]

In tissue, the principal scatterers are the cell nuclei, mitochondria, lysosomes and the Golgi apparatus. There is also a small contribution from the cell membranes. In fatty tissue, lipid vesicles (fat droplets) are important scatterers.[1]

In Figure 2.4, typical values of absorption and scattering in tissue are indicated for different wavelengths.

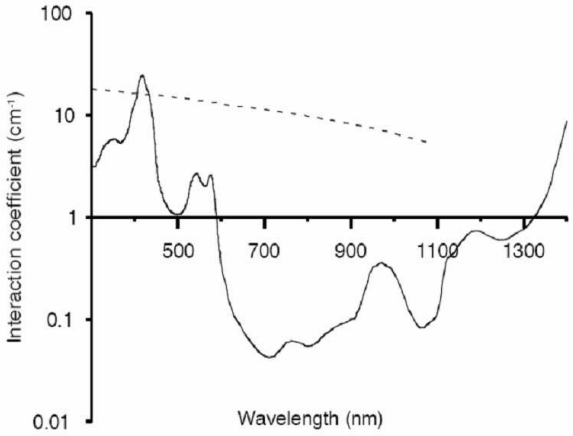

Figure 2.4: Typical scattering (dashed line) and absorption (solid line) coefficients for tissue, adapted from af Klinteberg.[10] The absorption is the sum of the absorption from oxygenated and deoxygenated haemoglobin (2/3 HbO_2 and 1/3 Hb) and water with a haemoglobin concentration of 1% and a water content of 70 %.

Scattering Phase Function

The scattering phase function, $p(\mathbf{s}, \mathbf{s}')$, gives the probability of scattering from direction $\mathbf{s}'$ into direction $\mathbf{s}$. If it is assumed that the tissue is isotropic in terms of refractive index, density and other physical properties, the phase function can be written as

$$p(\mathbf{s}, \mathbf{s}') = p(\mathbf{s} \cdot \mathbf{s}') = p(\cos\theta), \tag{2.4}$$

which is the same as saying that the scattering probability depends only on the angle, θ, between $\mathbf{s}$ and $\mathbf{s}'$ (it is then assumed that the scattering probability is symmetric for the azimuthal angle ψ). The scattering angles are illustrated in Figure 2.5.[5]

The phase function is normalized:

$$\int_{4\pi} p(\mathbf{s}, \mathbf{s}')dw = 2\pi \int_{-1}^{1} p(\cos\theta)d(\cos\theta) = 1. \tag{2.5}$$

Considering Mie theory, the scattering becomes increasingly forward-favoured as the particle diameter increases. Due to interference effects, lobes are visible in certain angles. But in tissue, which consists of a polydisperse ensemble of particles, the lobes average out and the phase function becomes more or less

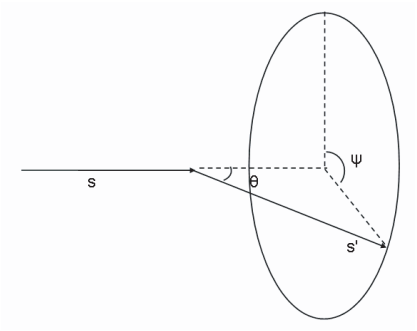

Figure 2.5: Definition of the scattering angles θ and ψ.

smooth. A phase function commonly used to approximate this shape is the Henyey-Greenstein phase function:[4]

$$p(\cos\theta) = \frac{1-g^2}{4\pi(1+g^2-2g\cos\theta)^{3/2}}. \tag{2.6}$$

Here, g is called the scattering anisotropy factor or the g-factor. It is the parameter usually employed in tissue optics to describe the angular distribution of the light scattering. The g-factor is defined as the expectation value of the cosine of the scattering angle θ:[5]

$$g = \frac{\int_{4\pi} p(\mathbf{s},\mathbf{s}')(\mathbf{s}\cdot\mathbf{s}')dw}{\int_{4\pi} p(\mathbf{s},\mathbf{s}')dw} = \int_{4\pi} p(\mathbf{s},\mathbf{s}')(\mathbf{s}\cdot\mathbf{s}')dw = <\cos\theta> . \tag{2.7}$$

For totally forward scattering medium the g-factor is 1 and for totally back scattering material it is -1. In the case of isotropic scattering g is equal to 0. For visible and NIR (near infrared) wavelengths in tissue the g-factor is between 0.7 and 0.99.[5] The Henyey-Greenstein phase function for different g-values is shown in Figure 2.6.

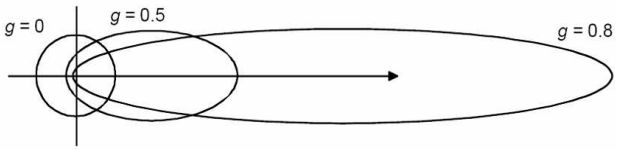

Figure 2.6: The Henyey-Greenstein phase function for different g-values. Adapted from Swartling.[4]

In tissue optics the reduced scattering coefficient μ_s' is frequently used. It is defined as

$$\mu_s' = \mu_s(1-g). \tag{2.8}$$

After a certain number of scattering events, the direction of a photon is almost independent of its initial bearing. In this case several unisotropic scattering

events with a mean free path length of $1/\mu_s$ can also be modelled by isotropic scatterings with a mean free path length of $1/\mu_s'$. This is known as the diffusion regime and light propagation is essentially described by isotropic diffusion.

2.1.3 The Beer Lambert Law

If light with intensity I passes through a sample, the difference in intensity, dI, can be expressed as[9]

$$dI = -I\epsilon c dz, \tag{2.9}$$

where dz $[m]$ is the sample thickness, c $[M]$ is the molar concentration and ϵ $[M^{-1}m^{-1}]$ is the molar extinction coefficient. This expression can then be integrated to

$$\ln\left(\frac{I}{I_0}\right) = -\epsilon c z \tag{2.10}$$

giving

$$I = I_0 e^{-\epsilon c z}. \tag{2.11}$$

The absorbance, defined using the natural logarithm, is then

$$A \equiv \ln\left(\frac{I_0}{I}\right) = \epsilon c z. \tag{2.12}$$

The absorbance could also be defined with the common logarithm ($\log_{10}$), as is often the case in e.g. chemistry. The relation between the concentration of an absorber and the corresponding absorption coefficient, μ_a, is given by[11]

$$\mu_a = \epsilon c. \tag{2.13}$$

2.2 Fluorescence

When the energy of a photon matches the energy difference between two energy levels in a molecule, the photon can be absorbed. The photon energy is then used to excite the molecule to a higher energy band, but since excited states are shortlived, the molecule will return to the ground state. This de-excitation can occur in several different ways, where emission of fluorescence light is one of the possible processes.

The fluorescence process is shown schematically in Figure 2.7. When a molecule is excited, it will not necessarily be excited to the lowest vibrational state in the excited electronic state due to the Franck-Condon principle.[12] From a vibrational state different from the lowest vibrational level there is a rapid relaxation to the lowest rotational-vibrational state within the upper electronic level. The de-excitation may occur through the emission of a photon by transferring the molecular energy from this level to the ground-state. This process is called fluorescence. The photon emitted in this way has less energy than the incoming photon, which means that the fluorescence light has a longer wavelength than the light causing the excitation.

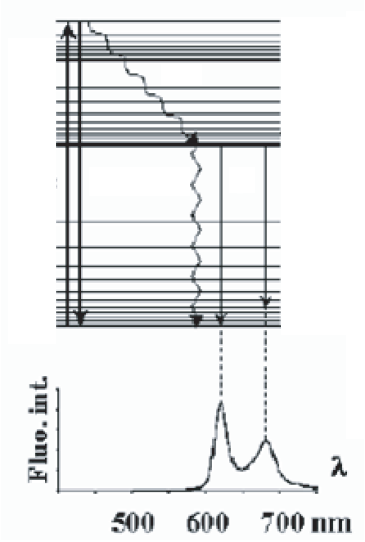

Figure 2.7: A schematic picture of fluorescence. In the lower part of the figure, an example of a fluorescence spectrum is shown. The figure is adapted from reference 12.

2.3 Fibre Optics

The use of optical fibres to transport light has increased considerably in recent years. Especially in communications the application of optical fibres is of great importance, but other areas, like laser medicine, are also dependent on the progress in this field. In the case of medical applications, fibre optics is an effective and practical way to transport light from the light source to the location of treatment or diagnostics and back to the detection equipment.[8]

2.3.1 Properties of Optical Fibres

An optical fibre is a transparent solid cylinder, e.g. a glass fibre, that has a refractive index that is higher than for the surrounding medium, which will lead to channelling of light through the fibre. This is illustrated in Figure 2.8, which shows a section of a fibre.

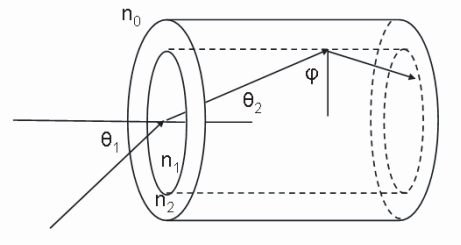

Figure 2.8: A ray incident on the core of an optical fibre.

Numerical Aperture

All incoming light will not be able to pass through to the other side of the fibre, since total internal reflection is required for the fibre to guide the light. This means that there is a maximum angle for the incoming ray, called the *acceptance angle*, that will lead to guidance of the light. For larger angles, photons will escape out of the fibre. The central part of the fibre, called the *core*, has a refractive index of n_1 and the encasing medium, called the *cladding*, has a refractive index of n_2. A medium with refractive index n_0 surrounds the fibre. The incoming ray is refracted as it hits the surface of the core according to

$$n_0 \sin\theta_1 = n_1 \sin\theta_2 \tag{2.14}$$

and the condition for total internal reflection is

$$n_1 \sin\varphi_c = n_2 \sin 90^\circ, \tag{2.15}$$

where φ_c is the critical angle. From Equations 2.14 and 2.15 the expression for the numerical aperture, NA, can be derived, which is a measure of how much light the fibre will accept. The larger the numerical aperture, the more light the fibre accepts.

$$\begin{aligned} \theta_2 &= 90^\circ - \varphi_c \\ \sin\theta_2 &= \cos\varphi_c = \sqrt{1-\sin^2\varphi_c} \\ NA &= n_0 \sin\theta_1 = n_1\sqrt{1-(n_2/n_1)^2} = \sqrt{n_1^2 - n_2^2} \end{aligned} \tag{2.16}$$

Modes

The acceptance angle is not the only criteria that has to be fulfilled for a ray to propagate successfully through the fibre. Considering the wave properties of light, only certain ray directions or *modes* are allowed. The light directions propagating in the fibre can be seen as the result of constructive interference between an incident light wave and the same wave reflected twice at the core-cladding interface. From the mode structure, two basic fibre types can be defined: multimode fibres that permit a discrete number of modes to propagate and single mode fibres that are thin enough so that only one mode is allowed. A larger fibre diameter allows more modes to oscillate.[8, 13]

Fibre Types

The fibre type shown in Figure 2.8 above, where the core is homogeneous with a single index of refraction, is called *step-index* fibres because of the discontinuous change in refractive index between core and cladding. Another type of fibre is the *graded index* fibre, where the index of refraction decreases continuously from the core central axis as a function of radius.[8]

Attenuation

As light propagates through the fibre the intensity will be attenuated due to several different mechanisms. Among the extrinsic losses are losses due to inhomogeneities in the fibre and geometric effects, like e.g. sharp bends. Light is also lost as it is coupled into and out of the fibre. Intrinsic losses are due to absorption and scattering in the core. The attenuation is characterized by the *attenuation coefficient*, α, and is given in decibels.

$$\alpha_{dB} = 10 \log_{10} \left(\frac{P_1}{P_2} \right) \tag{2.17}$$

P_1 and P_2 are the power of the light at the input and output surfaces of the fibre.[8]

Distortion

Light transmitted through a fibre will undergo pulse broadening, due to distortion of the wave. The major causes of distortion are, in order of decreasing severity, mode dispersion, material dispersion and waveguide dispersion. Mode dispersion is due to different propagation velocities for different modes. The axial ray travels the shortest way through the fibre and arrives first at the output, whereas the ray propagating at the critical angle experiences the longest distance. Material dispersion is caused by the fact that the refractive index is a function of wavelength. Each wavelength component has a different refractive index and consequently propagates at a different speed. The waveguide dispersion is a small effect that depends on the ratio between the core radius and the wavelength of the light.[8]

2.4 Measuring Optical Properties

In many applications it is desirable to find the optical properties of tissue *in vivo*, e.g. its scattering and absorption. This can be done by measuring the light either transmitted through or scattered back by the tissue. Different combinations of scattering and absorption usually give very similar signals. For instance, a reduced detected signal can be either due to an increase in absorption or a longer photon path caused by a change in the scattering. To be able to measure both scattering and absorption simultaneously, the measurement can be either spatially resolved, time-resolved or frequency-resolved. These methods are illustrated in Figure 2.9 and further described below. They can be used to measure μ_s' and μ_a, but none of them can separate μ_s' into μ_s and g.[4]

2.4.1 Spatially Resolved Measurements

Spatially resolved measurements, as shown in Figure 2.9 (a), are usually performed using continuous light sources and are then referred to as continuous

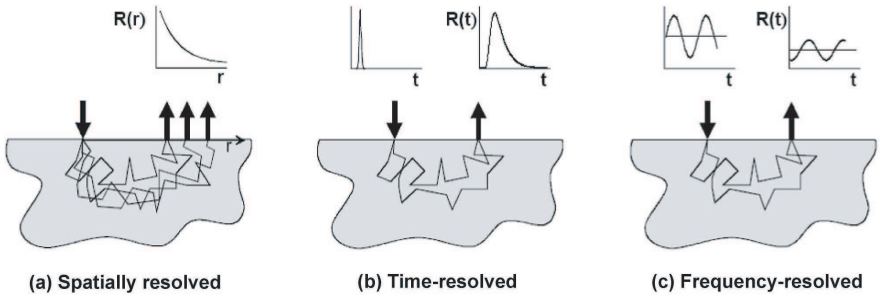

Figure 2.9: Three ways to measure μ_s' and μ_a: (a) spatially resolved, (b) time-resolved and (c) frequency-resolved techniques. The figure is adapted from Eker.[14]

wave (CW) or steady-state measurements. The sensitivity to μ_s' and μ_a varies with the distance between the source and the detector. The two parameters can thus be separated using only two source-detector separations, but the determination is more robust if more separations are used. The equipment for spatially resolved measurements is relatively inexpensive and portable, but suffers from sensitivity to inhomogeneities in the medium.[4]

2.4.2 Time-Resolved Measurements

Another way to measure μ_s' and μ_a is to send a short pulse in the order of picoseconds into the tissue and measure the temporal shape of the detected signal. The pulse is stretched in time, because the photons are scattered in the tissue and follow paths of different lengths. The late photons have taken long paths through the tissue and are thus very sensitive to absorption. The early photons on the other hand have taken shorter paths and are less sensitive to absorption. Instead they carry more information about the scattering. The more the photons have been scattered around, the later they arrive. In this way μ_s' and μ_a can be derived using the early and the late part of the signal respectively. To get more accurate values for the optical properties, theoretical or simulated curves can be fitted to the measured temporal signal. Compared to spatially resolved measurements, time-resolved measurements are less affected by small inhomogeneities, but the equipment is more expensive and complicated.[4]

2.4.3 Frequency-Resolved Measurements

In frequency-resolved measurements, the intensity of the light source is sinusoidally modulated with a frequency of typically some hundreds of MHz. Each individual photon is scattered back and forth in the tissue and coherence is quickly lost, but macroscopically a diffuse photon wave is propagating spherically out from the light source. This wave has a well defined amplitude and phase for many centimetres. The amplitude and phase are affected by the optical properties of the tissue and if they are detected, μ_s' and μ_a can be cal-

culated. The frequency-resolved method is mathematically equivalent to the time-resolved method and they are related by a Fourier transform.[14]

2.5 Measuring the Absorption Coefficient (μ_a)

For some applications, one is only interested in the absorption. Instead of performing a spatially resolved measurement, it could in principle be sufficient to conduct a continuous wave measurement at only one source-detector separation. The separation should be chosen so that the measurement is invariant to variations in scattering.[4] This separation is specific for a certain geometry, measurement method and range of optical parameters. Depending on the selected measurement method, either the detected intensity[15] or the effective photon path length[2,3] (as defined below) should be invariant. Both cases are discussed in the following paragraphs.

2.5.1 The Effective Photon Path Length (L_{eff})

Diffuse reflectance, as illustrated in Figure 2.10, can be used to measure the change in absorption coefficient $\Delta\mu_a$. Light with intensity I_{in} is sent into the tissue and an intensity I is detected. To evaluate I, it has to be compared to a calibration measurement, I_0, denoting the detected signal before the absorber is added. I_0 depends on geometry, scattering and background absorption. Changes in absorption then affects I according to the Beer Lambert law, as explained in Section 2.1.3.[2,3]

$$I = I_0 e^{-\Delta\mu_a L_{eff}} \tag{2.18}$$

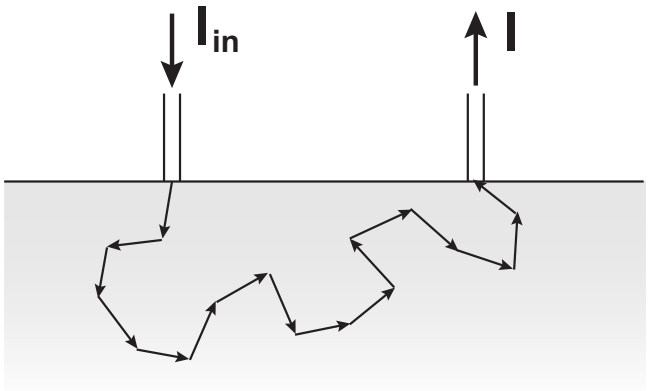

Figure 2.10: Measurement geometry for diffuse reflectance measurements where an intensity I_{in} is sent into the tissue and the intensity I is detected. Usually, fibre optics is used to deliver and detect the light.

What is then L_{eff} in this formula? When optical properties are measured in a non-scattering medium, all photons travel the same distance, which is then

also the distance in the Beer Lambert law. In the case of scattering media, the different photons are scattered differently and thus follow paths of different length. To use the average path length in the evaluation would not yield the right answer, because of the exponential dependence. The L_{eff} entering Equation 2.18 is instead the effective path length that can replace the full path length distribution in the Beer Lambert law.[2,3]

$$L_{eff} = -\frac{ln\left(\frac{I}{I_0}\right)}{\mu_a} = \frac{ln\left(\frac{I_0}{I}\right)}{\mu_a} \tag{2.19}$$

2.5.2 The Magic Distance (invariant L_{eff})

If I_0 and I are measured and L_{eff} is known, then $\Delta\mu_a$ can be calculated from Equation 2.18. L_{eff} can be found through measurements or simulations, but varies widely with the scattering. In the case of one source-detector pair, there should, however, be one inter-fibre separation where the variation of L_{eff} with scattering is minimal. This separation is denoted the *magic distance* and its existence can be explained by the following, illustrated by Figure 2.11.[2,3]

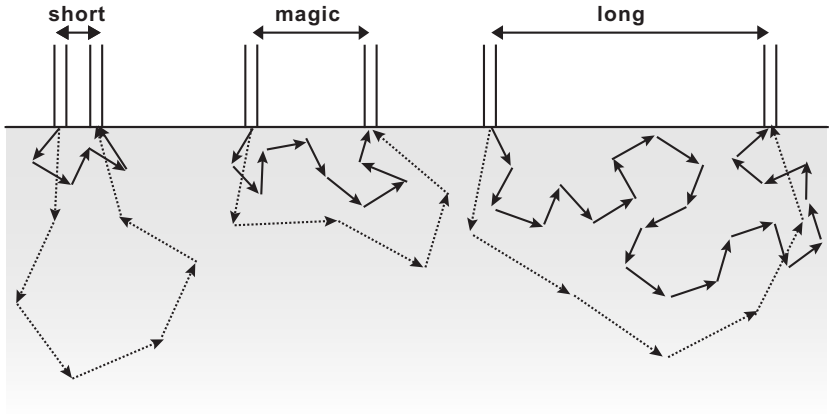

Figure 2.11: Examples of how photons might travel for three different source-detector separations. The short solid arrows represent high scattering whereas the longer broken arrows represent low scattering. The length of the arrows and the scattering angels are exaggerated for clarity.

When the diffuse reflectance is measured, the photons have to be scattered sufficiently many times to turn 180° and return to the detector. If the source-detector separation is *short*, then photons have to travel further to be scattered enough times the *lower* the scattering. If, on the other hand, the source-detector separation is *long*, the photons soon lose track of their original direction and follow a zigzag path that is longer the *higher* the scattering. Somewhere in between these two extremes there should be a source-detector separation where the two effects cancel and the effective path length varies minimally with the scattering. This separation is the magic distance.[2,3]

The magic distance phenomenon has been demonstrated for diffuse surface reflectance measurements by Mourant *et al* through both Monte Carlo simulations

and measurements on tissue phantoms.[3] The optimum source-detector separation was found to be approximately 1.7 mm for the range of optical properties usually encountered in tissue. This separation was used to measure unknown concentrations with an accuracy of 20 %. The same method was also used to measure tissue concentrations of chemotherapy agents.[2] In this project we extend the magic distance concept to interstitial measurements.

2.5.3 The Pivot and Hinge Points (invariant intensity)

There is another concept, similar to the magic distance, known as pivot and hinge points, illustrated by Figure 2.12. These are the source-detector separations where the detected intensity (not L_{eff} as in the previous paragraph) is invariant to scattering and absorption respectively.[15]

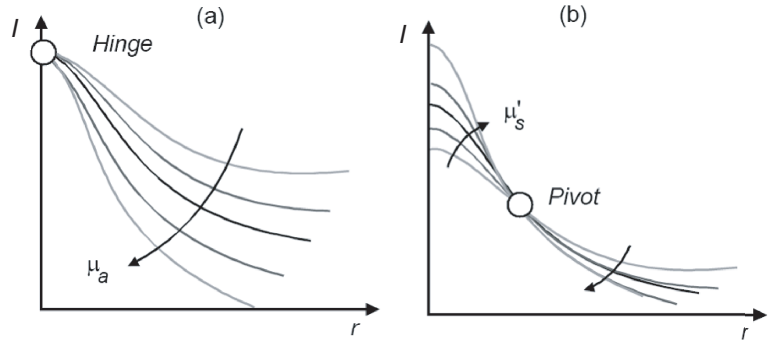

Figure 2.12: The figures show detected intensity I for different source-detector separations r. (a) illustrates the hinge point where the detected intensity is invariant to changes in absorption and (b) the pivot point where the detected intensity is the least dependent on scattering. The figures are adapted from Dam.[15]

For *short* source-detector separations, light is reflected back to a higher degree the higher the scattering. For *long* separations, less light manages to diffuse all the way to the detector the higher the scattering. At a certain distance, known as the pivot point, these two effects cancel and the detected intensity depends minimally on the scattering. According to experiments, this distance is approximately 3 mm for the range of optical parameters usually found in tissue. Theoretically, this should be a good source-detector separation to measure the absorption coefficient independently of the scattering, but experimentally a combination of measurements at shorter and longer distances yields a higher robustness and accuracy.[15]

If one, on the other hand, wants to measure scattering independent of absorption, it is desirable to use as short source-detector separation as possible, because the light is less affected by absorption the shorter it travels through the tissue. This can be seen as a *hinge point* in Figure 2.12 (a).[15] This principle is also used in elastic scattering spectroscopy (ESS), which is a method where a probe with fibres close to each other measures mainly the scattering properties of the tissue.[16–18]

2.5.4 What Is the Difference?

The two concepts - the magic distance and the pivot point - might seem very similar. The difference is that the *effective path length* is invariant to scattering at the magic distance, while the *detected intensity* is invariant at the pivot point. This is not the same thing. Even though the same amount of photons might reach the detector at the pivot point when the scattering is varied, their effective path length might be different.

Then how do you know which source-detector separation to choose? It simply depends on the measurement situation. Both methods need calibration, but in different ways. If the magic distance is used, the measured intensity, I, is compared to the corresponding intensity before any change in absorption, I_0. If the pivot point is used, then the detected intensity I is compared to the intensity I_{in} entering the tissue and provided a measured or simulated calibration curve, I_{in} is related to an absorption coefficient. Both methods have their advantages and disadvantages and they are suitable in different situations.

2.6 Monte Carlo Simulations

The Monte Carlo method is a stochastic model based on random walk and it is a method frequently used to simulate light transport in tissue. Using this model, a photon or photon package is traced through the tissue until it exits the geometry or is terminated due to absorption. Statistics of the physical quantities are obtained by repeating the tracing for a large number of photon packages, where the number of photons needed depends on the problem and the wanted accuracy. The main steps in a Monte Carlo simulation are shown in the flow chart in Figure 2.13. The theory in this section is mainly based on that presented by Prahl et al.[19]

2.6.1 Photon Initialization

The simulation starts when a photon is given a position and a direction and is launched into the tissue. The properties of the initialized beam can be varied: if a collimated beam is simulated, the photon is initialized in a chosen direction into the tissue and if a diffuse irradiance is modelled, the photon's direction is chosen randomly etc. One way to improve the efficiency of a Monte Carlo program is to propagate a photon packet instead of a single photon. This means that instead of following one photon until it is absorbed or exits the medium, a packet of photons is traced and a portion of the packet will be absorbed at each step. The size of the packet is called the photon weight (w) and is initially set to unity.

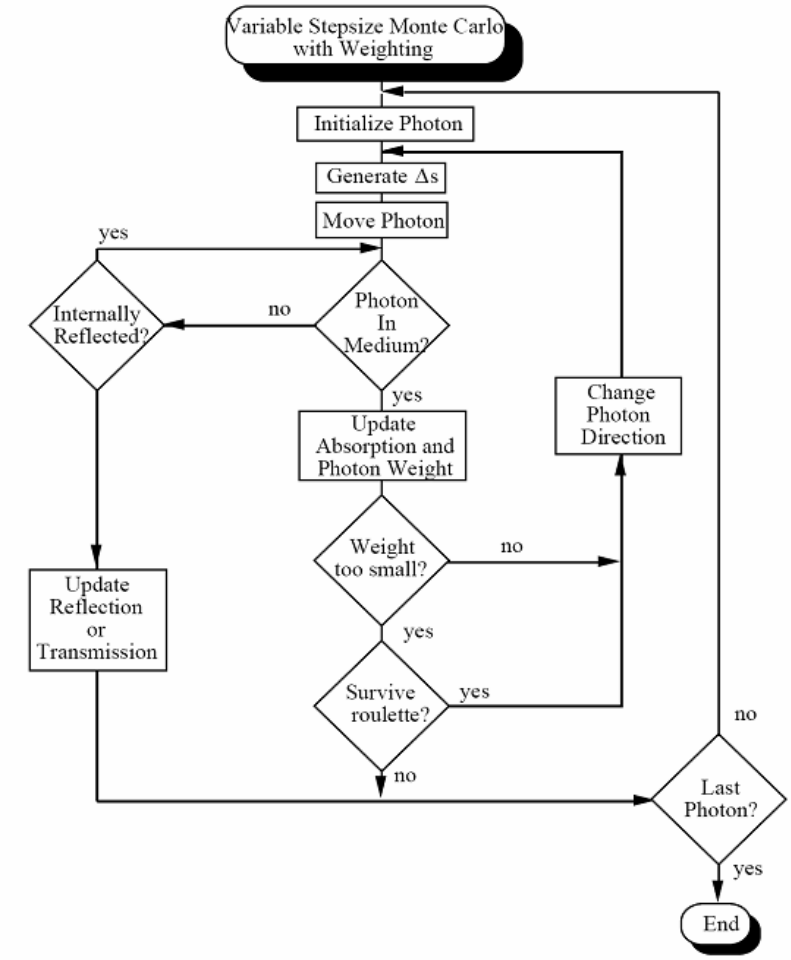

Figure 2.13: Flowchart of the Monte Carlo technique from Prahl.[19]

2.6.2 Moving the Photon

In the most simple case a small, fixed incremental step size is used to propagate the photons. The step size Δs must then be small in comparison to the average mean free path length of a photon in the tissue:

$$\Delta s << \frac{1}{\mu_t} = \frac{1}{\mu_s + \mu_a}. \tag{2.20}$$

If the step size is too small the photon will hardly interact with the tissue and the simulation will be inefficient. If the step size is too large the distance travelled by the photon will not be a good approximation of the real case. To increase the efficiency, different step sizes could be chosen for each step. Since the attenuation is exponential and follows Beer's law, the probability is proportional to $e^{-\mu_t \Delta s}$. Thus, it can be related to a random number, ξ, distributed between zero and

one by

$$\Delta s = \frac{-\ln \xi}{\mu_t}. \tag{2.21}$$

Now the average step size will be $1/\mu_t$, since the statistical average of $-\ln(\xi)$ is one. This step size represents the average distance a photon will travel before interacting with the tissue.

The direction of the photon could be specified by three direction cosines, which are obtained by taking the cosine of the angle that the photon's direction makes with each axis. The new coordinates are then given by

$$\begin{aligned} x' &= x + \mu_x \Delta s \\ y' &= y + \mu_y \Delta s \\ z' &= z + \mu_z \Delta s \end{aligned} \tag{2.22}$$

where μ_x, μ_y, μ_y are the direction cosines, (x, y, z) is the original position and (x', y', z') is the new position of the photon.

If the photon hits a boundary within the calculated step size, it is moved to the boundary and the angle of incidence, θ_i, and the angle of transmission, θ_t, are calculated. The angle of incidence is $\theta_i = \cos^{-1} \mu_z$ and the angle of transmission is given by Snell's law, $n_i \sin\theta_i = n_t \sin\theta_t$. The probability that the photon will be internally reflected is determined by the Fresnel reflection coefficient, see Equation 2.2. A random number, ξ, uniformly distributed between zero and one is used to decide whether the photon is reflected or transmitted. If $\xi < R$, the photon is internally reflected, otherwise the photon exits the tissue.

2.6.3 Absorption and Scattering

After each step taken by the photon packet, one fraction will be absorbed and the rest will be scattered. The fraction absorbed is

$$frac_{abs} = \frac{\mu_a}{\mu_a + \mu_s} = 1 - \frac{\mu_s}{\mu_a + \mu_s} \tag{2.23}$$

which means that the weight should be decreased by

$$w \frac{\mu_a}{\mu_a + \mu_s} = w \frac{\mu_a}{\mu_t} \tag{2.24}$$

in every interaction event. The weight of the packet that is scattered is thus given by

$$w' = w \left(1 - \frac{\mu_a}{\mu_t}\right) = w \left(\frac{\mu_s}{\mu_t}\right). \tag{2.25}$$

Both the position of the absorption event and the amount of light being absorbed are recorded for the analysis.

After each step taken, the photon is being scattered, which means that it changes direction. In tissue, scattering is often described by the Henyey-Greenstein phase function, see page 8. In this case the scattering angle θ is given by

$$\cos\theta = \frac{1}{2g} \left(1 + g^2 - \left[\frac{1 - g^2}{1 - g - 2g\xi}\right]^2\right). \tag{2.26}$$

This is not valid for an isotropic distribution, i.e. when $g = 0$, in this case the scattering angle is instead defined by

$$\cos\theta = 2\xi - 1. \tag{2.27}$$

If the phase function has no azimuthal dependence, which is the case for the Henyey-Greenstein phase function, the azimuthal angle is uniformly distributed between 0 and 2π. It can then be calculated according to

$$\phi = 2\pi\xi. \tag{2.28}$$

2.6.4 Photon Termination

When using photon packets, the weight will decrease during each absorption event, but in principle it will never reach zero. This will make the simulation impossible, since following very small packets will yield very little information and one would never reach the initialisation of the next photon package. To kill all packets that have reached a certain minimum weight is not a good idea, since this will violate the conservation of energy. Instead a method called roulette is used to terminate the photons. Every packet whose weight drops below a minimum is given the probability $1/m$ (e.g. $1/10$) of surviving with a weight mw. If it does not survive its weight is reduced to zero.

2.6.5 White Monte Carlo

One way of reducing the number of computations needed for Monte Carlo simulations is to perform only one simulation with $\mu_a = 0$. The absorption is then added afterwards using the Beer Lambert law. This method, known as white Monte Carlo will, however, result in slightly different photon distributions as compared to the conventional method because of the different step sizes. The conventional step size is, on average, $1/\mu_t$ whereas it is $1/\mu_s$ with the white method. There will also be a difference in how the photon weights are handled. In the conventional approach the weight is decreased according to Equation 2.24 in each interaction event, which means that after N steps the packets have, on average, travelled, a distance $d = N/\mu_t$ and have a weight

$$w_d = w\left(1 - \frac{\mu_a}{\mu_t}\right)^N. \tag{2.29}$$

The corresponding weight for a white simulation after the same distance would be

$$w' = we^{-d\mu_a} = we^{-N\frac{\mu_a}{\mu_t}}, \tag{2.30}$$

here N still is the number of steps in the conventional simulation. In the white simulation the number of steps would be different.

In tissue optics problems the absorption is usually much smaller than the scattering, which is the same as saying that the albedo $a = \frac{\mu_s}{\mu_a+\mu_s} \to 1$. In this case the two different step sizes become very similar and it can be shown with Taylor expansion that the white approach is equivalent to the conventional.[4]

Chapter 3

Methods and Equipment

Both simulations and experiments were used to evaluate the design, in the development of a catheter with optical fibres. The theoretical data from the simulations and the experimental results were then compared. This requires that the optical properties of the tissue are known. According to a study of the optical properties of human prostate tissue made by Svensson *et al*,[20] μ_s' is 9±2 cm^{-1} and μ_a is 0.5±0.1 cm^{-1} at 660 nm and these are the values used both in the simulations and the experiments. To be able to fit the two fibres into a brachytherapy needle, fibres with a core diameter of 300 μm were used.

3.1 Simulations

3.1.1 The ASAP Software

ASAP is an abbreviation for "Advanced Systems Analysis Program" and is a software for analysis of light propagation developed by Breault Research. It is a program well suited to perform the simulations in this project. Unlike many other ray-tracing programs, ASAP can handle scattering. Compared to other simulation programs that use the Monte Carlo technique, e.g. MCML, the possibility to create any 3D geometry and build complicated systems is a great advantage. On the other hand, the complexity makes it harder to learn how to take advantage of all different possibilities in the program. A disadvantage with ASAP is the very long simulation times necessary to collect enough data for a statistical analysis using the Monte Carlo technique.

ASAP is one of few ray-tracing programs that is able to simulate volume scattering, which is necessary when modelling light propagation in tissue. There are two different kinds of ray-tracing: sequential and non-sequential. In sequential ray-tracing the program only traces rays that follow a pre-defined path, i.e. the rays encounter the objects, such as lens surfaces, in a prescribed order. By ignoring other rays the evaluation can be made faster. In non-sequential ray-tracing, all rays are followed, which is a requirement when dealing with scattering mate-

rials. In ASAP rays can automatically split into reflected, refracted, diffracted, polarized and scattered components as they propagate through the system. The rays propagate independently, encountering objects in any order, as appropriate. ASAP is also able to simulate coherence and diffraction using a method called Gaussian beam decomposition.[21]

The simulated system can be created in two different ways. Either with the "builder", which is a user-friendly interface where the user more or less is told which parameters to define, or with the more powerful script language. Three different parts have to be defined. The first part consists of parameters such as wavelength, units and materials. The second part is where the geometry, consisting of different objects, is created. Each object is defined by its shape, location and dimensions. The last section consists of the light sources, the ray trace and the analysis. An example of the interface, including a part of a script used in the simulations, is shown in Figure 3.1.

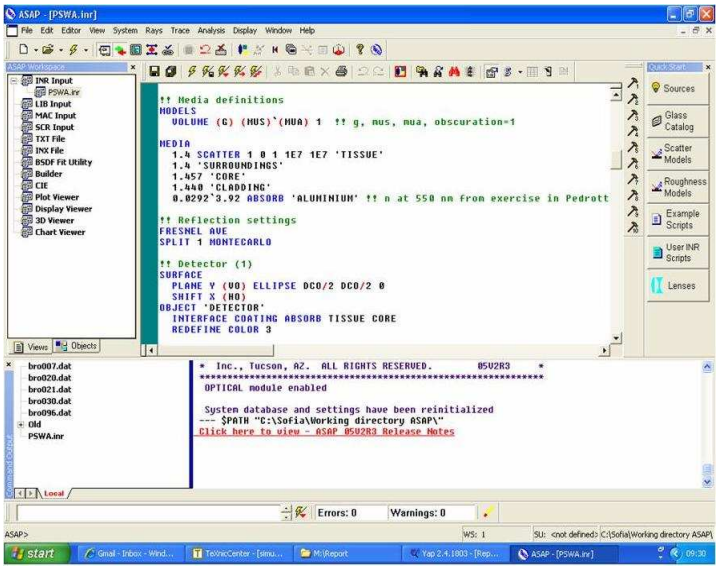

Figure 3.1: Example of the ASAP interface, including a part of a script used in the simulations.

Modelling Scattering Media

In ASAP, a volume scatter medium can be modelled in different ways. Either with the Mie particles model where scattering spheres are distributed throughout the volume, or with a Monte Carlo scatter using the Henyey-Greenstein phase function described in Section 2.1.2. In the first case the refractive index of both the bulk material and the scattering particles must be specified. For the

second method g, μ_s and μ_a should be provided.[22]

Rays and Ray-tracing

A ray in ASAP should not be confused with a photon, instead it can be considered to be composed of many photons. In ASAP, a ray is a point in space with associated direction and flux, defined in terms of three Cartesian coordinates and a direction vector. It represents a continuous delivery of power, which means that a ray can simulate a local flow of electromagnetic energy. As a consequence, a simulation represents a steady-state situation, i.e. there is no time-dependence.

As stated above, the rays propagate independently through the system and encounter objects in the order that is physically appropriate. Rays in ASAP always belong to objects. When a ray is created it is assigned to a fictitious object and during the trace it is instantaneously moved from one object to another. After the ray-trace is finished, the rays always belong to the object it intersected last.

A source in ASAP is basically a collection of rays that can have any shape and consist of any number of rays. It is also possible to create a certain beam profile, like e.g. a Gaussian.

There exist both numerical and graphical tools to analyse the result in ASAP. For each ray, it is possible to get information on final position, direction and which object it belongs to, i.e. the last object it intersected. Other examples of information that is registered are the flux and the path length travelled by each ray. It is also possible to plot the rays as they propagate through the system during the trace, which gives a picture of the ray paths. In the analysis either all rays can be accounted for, or only rays that fulfil certain criteria, e.g. belong to a certain object or carry a certain flux.

There are several reasons as to why rays might be terminated during the trace. Ideally the rays will stop when they reach an absorbing surface, which is a surface defined with zero reflection and transmission, but this is not always the case. A ray can stop because the flux is so low that it has reached a flux threshold or because it has interacted with too many objects, parameters that can be changed by the user. Another reason could be that a ray has been traced to an object with non-zero transmission or reflection coefficient and finds no other object along its path.[21]

3.1.2 The Model

An example of our ASAP code is shown in Appendix B and the geometry of the model can be found in Figure 3.2. A sphere with a radius of 2.5 cm and refractive index of 1.4 was used to simulate the prostate tissue. Two optical fibres with a core diameter of 300 μm, cladding thickness of 15 μm and jacket thickness of 35 μm were positioned side by side in the middle of the sphere, see

Figure 3.3. The length of the fibres was 6 cm.

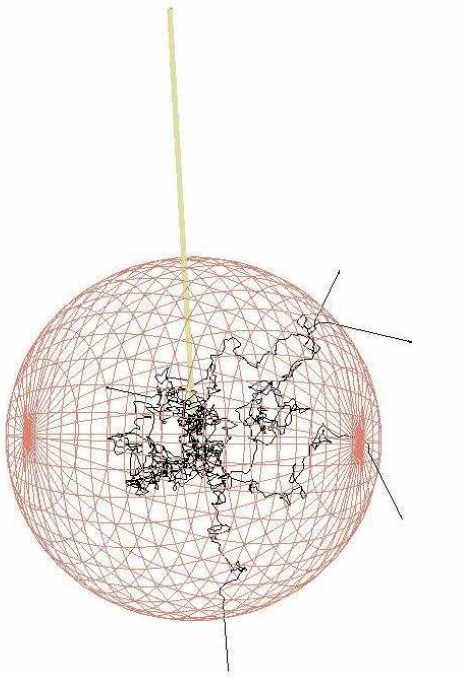

Figure 3.2: The geometry used to model the probe with two optical fibres (yellow) in the prostate gland (pink). The black lines are examples of paths taken by rays.

The parameters that were changed between different simulations in order to find the optimal vertical offset between the fibres were the scattering coefficient in the volume scatter model and the vertical offset between the source and detection fibres, see Figure 3.4.

The photons that did not reach the detector were terminated in different ways. The surface of the sphere was 100 % transmitting and the surrounding medium had the same refractive index as the sphere. Thus all rays that hit the sphere were transmitted and terminated. If the total number of scattering events for one single ray reached a certain limit, the ray was killed. This limit was predefined to 1000 and this was the limit used in our simulations, but if desired it is possible to change. It is also possible to define a flux threshold, but in this model white Monte Carlo was used, i.e. the absorption in the volume scatter models was set to zero, in order to decrease the simulation time. This means that the flux was not affected during the trace. The simulation time varies depending on the values of the different parameters, but typically only 0.002-0.03 % of the launched rays were detected in our model.

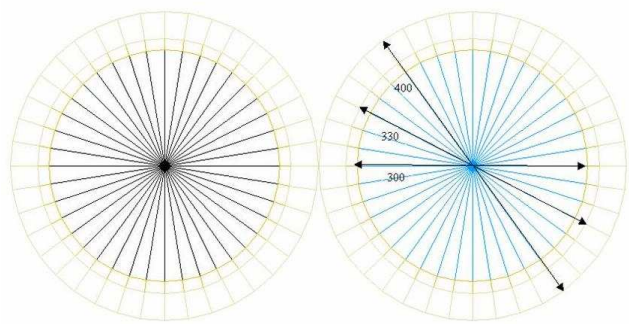

Figure 3.3: A schematic figure of the source (black) and detector (blue) fibres. The core is 300 μm in diameter, the cladding thickness is 15 μm and the jacket thickness is 35 μm.

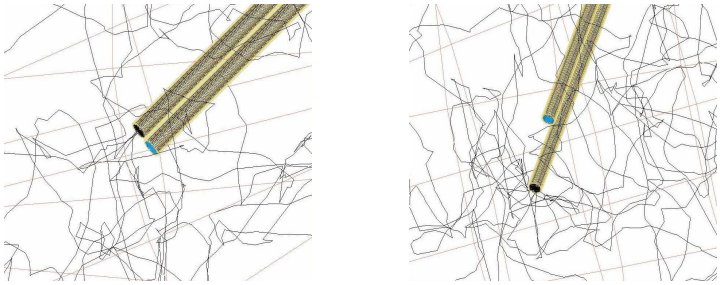

Figure 3.4: The source (black) and detector (blue) fibres. The left figure shows the fibres without a vertical offset and the right figure shows the fibers with a vertical offset of 2 mm.

When analysing the result, only the rays absorbed on the detector were considered. In order to account for the numerical aperture of the fibre, only the rays incident on the detector within the numerical aperture of the detection fibre were analysed. The numerical aperture for the simulated fibres was 0.22, which gives a detection angle of 9.04° in tissue with a refractive index of 1.4. The interesting parameters collected for analysis were the flux and the optical path length (OPL).

3.1.3 Data Analysis in Matlab

From the simulations, information on the optical path length was collected and analysed in Matlab. Since the simulations were performed without absorption, the absorption was added afterwards in Matlab using the Beer Lambert law (see Section 2.1.3). The final flux for every ray used in the analysis was calculated from the initial flux, ϕ_0, which was the same for all rays, and the optical path length, OPL, travelled by the individual rays according to

$$\phi = \phi_0 \cdot e^{-\mu_a OPL/n} = \phi_0 \cdot e^{-\mu_a L}. \tag{3.1}$$

The parameter n is the refractive index of the tissue, in our case 1.4. This information was then used to calculate the effective path length described in Section 2.5.1. The calculation of the effective path length with standard error can be found in Appendix A.

3.2 Measurements

In order to experimentally evaluate the sensitivity of absorption measurements to scattering, liquid phantoms with known levels of absorption and scattering were used. The scattering and absorption coefficients of the phantom and the vertical offset between the emission and detection fibres were all varied and transmission signals between source and detection fibres acquired. The data was then evaluated to find out at which vertical offset the determination of the concentration was least influenced by the scattering. The setup, phantom, measurement sequence and data evaluation are described below.

3.2.1 Instrumentation

The experimental setup is illustrated schematically in Figure 3.5 and its appearance can be seen in Figure 3.6. A pulsed Xenon short-arc lamp was used as light source. Its spectrum is shown in Figure 3.7. The light was delivered to and collected from the phantom by 300 μm aluminium jacketed quarts fibres (Fiberguide Industries Inc., Sterling, New Jersey, AFS300/33A). The tip of the source fibre was positioned in the centre of the phantom, parallel to and in contact with the detection fibre. The detection fibre could be moved vertically with an accuracy of 0.01 mm. Both fibres and the needle holding them together can be seen in Figure 3.8 (a). The collected light was dispersed and detected by a

S2000 miniature spectrometer (Ocean Optics Inc., Dunedin, Florida). Both the lamp, spectrometer and controlling computer were built into a biospectrometer (Optimum Technologies Inc., Massachusetts, OPS-1000 Biospectrometer). A spectrally flat diffuse reflector based on Spectralon material (Lab Sphere Inc., Cranfield, UK) was used to measure the lamp spectrum before each set of measurements.

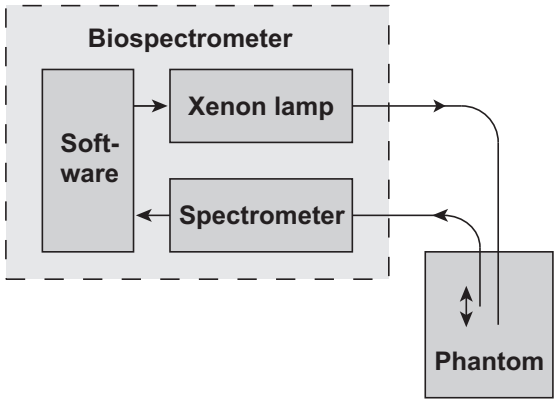

Figure 3.5: Schematic illustration of the setup. The detection fibre can be moved vertically.

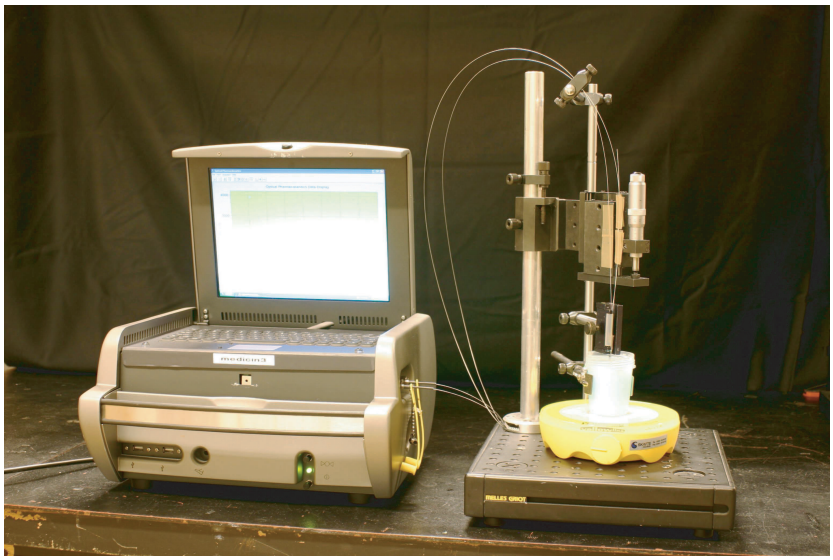

Figure 3.6: The experimental arrangement with the phantom to the right and the biospectrometer containing light source, spectrometer and computer to the left.

3.2.2 Phantom

To simulate the scattering properties of prostate tissue, an Intralipid solution (Fresenius Kabi, Uppsala, Sweden) was used. Intralipid is a fat emulsion used

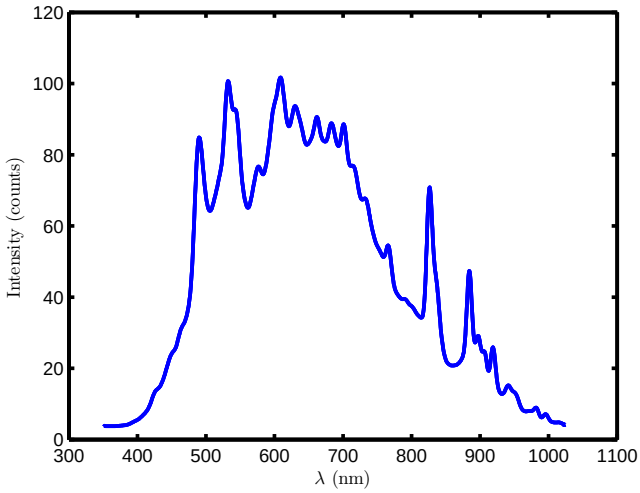

Figure 3.7: The spectrum of the Xenon short-arc lamp measured with the biospectrometer and Spectralon reference.

as intravenous nutritional supplement. Because of its scattering properties, it is often used as tissue phantom for optical experiments. Its scattering varies with wavelength, but the values in this text refers to the scattering at 660 nm. A blue dye, Methylene Blue hydrate (Sigma-Aldrich, St. Louis, Missouri), was added to the solution to give a detectable absorption peak. Its absorption spectrum is shown in Figure 3.9. In this work, the absorption peak at 668 nm was used. The Intralipid solution was kept in a 100 ml beaker (height 5 cm and minimum diameter 4.5 cm), big enough for boundary effects to interfere minimally with the measurements. All measurements were performed with the phantom at room temperature not to let temperature variations affect the measurement. Between measurements, the liquids were stored in a refrigerator. The appearance of the phantom can be seen in Figure 3.8 (b).

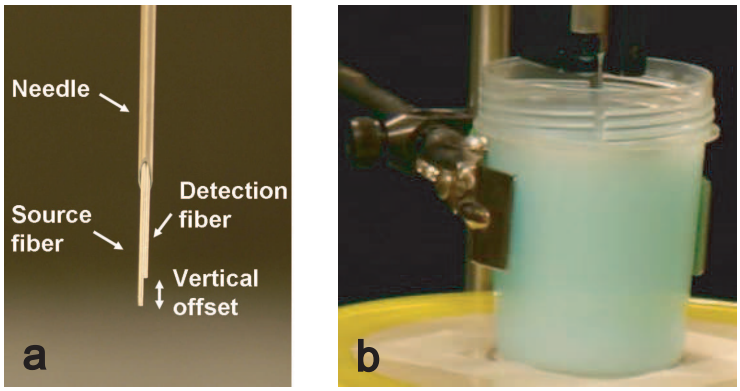

Figure 3.8: The needle with optical fibres (a) and the phantom (b). Here, the vertical offset between source and detection fibre is approximately 2.6 mm.

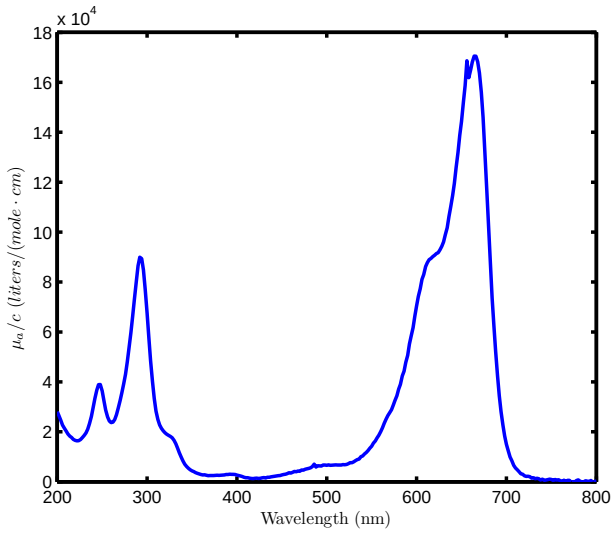

Figure 3.9: Absorption spectrum of Methylene Blue measured by Prahl.[23]

3.2.3 Measurement Sequence

In order to identify the vertical offset between source and detection fibre where the measured concentration depended the least on scattering, parameters such as vertical offset, absorption and scattering were varied. Measurements were performed at three different levels of scattering, $\mu_s' = 9$ cm^{-1}, the average scattering for prostate tissue, and $\mu_s' = 6$ cm^{-1} and $\mu_s' = 12$ cm^{-1} representing the maximum variations encountered.[20] For each scattering, the blue dye was added to increase the absorption peak in steps of 0.1 cm^{-1} from $\mu_a = 0$ cm^{-1} to $\mu_a = 0.8$ cm^{-1}. The diffuse reflectance was then measured for different vertical offsets in steps of 0.2 mm from 0 to 3 mm and thereafter in steps of 0.5 mm up to 8 mm.

3.2.4 Data Evaluation

For each combination of μ_s', μ_a and vertical offset, a spectrum was recorded. The spectra were then analysed in Matlab in order to evaluate the absorption imprint for each phantom measurement. First, all spectra were divided with a reference spectrum acquired from the spectralon reflection standard to distinguish the signal from the tissue phantom from the lamp spectrum. Then, the absorbance, as defined from the Beer Lambert law (Section 2.1.3), was calculated for each spectrum:

$$A(\lambda) = -\ln\left(\frac{I}{I_0}\right). \tag{3.2}$$

For a phantom with a certain scattering and vertical offset between the fibres, I_0 is defined by the measurement with no absorption present, i.e. when $\mu_a = 0$, and I is the measured intensity from the measurement to be evaluated. To account

for fluctuations in the lamp intensity the spectra were normalized. This was done by setting I equal to I_0 for the wavelength where Methylene Blue absorbs the least. In this way, I was always kept smaller than or equal to I_0, which should be the case since the addition of an absorber will cause a decrease in signal strength.

In the next step, a curve was fitted to the absorbance spectra using singular value decomposition (SVD). SVD is a method employed to factorize matrices providing a good fit of a linear combination of basis spectra to a data set. The SVD algorithm was used to fit the extinction coefficients of relevant absorbing components to the calculated absorbance spectra. The absorbers used were Methylene Blue and water, together with a set of free parameters to account for autofluorescence in the liquid phantom and offsets in the lamp spectrum. The set of free parameters used in this work consisted of a fourth order polynomial in wavelength, as this polynomial order was shown to yield a good fit to the experimental data. For each absorption spectrum, the SVD algorithm returned the different absorber concentrations, or more accurately $c \cdot L_{eff}$, where c is the concentration of a certain absorber in molar (M). This is related to the absorption coefficient through

$$\mu_a \cdot L_{eff} = \epsilon \cdot c \cdot L_{eff}. \tag{3.3}$$

In the evaluation it has been assumed that L_{eff} does not depend on μ_a, which is not altogether true. There is a dependence of L_{eff} on μ_a, which also means that L_{eff} varies with the wavelength, since μ_a is wavelength dependent. However, this effect was ignored as our experimental work only aimed at identifying the parameter $c \cdot L_{eff}$ and its dependence on variations in μ_s'.

Chapter 4

Results

4.1 Simulations

For each scattering and vertical offset between the source and detector, at least 850 rays were simulated and their path lengths recorded. From that, the effective photon path length (as defined in Section 2.5.1) and the detected flux were calculated. If nothing else is mentioned, these parameters were evaluated for $\mu_a = 0.5$ cm^{-1}.

4.1.1 The Effective Photon Path Length (L_{eff})

To be able to measure concentration independent from scattering we wanted to find the magic distance where the effective photon path length, L_{eff}, varies the least with respect to scattering (as explained in Section 2.5.2). L_{eff} and its standard error were calculated from the simulated path lengths as outlined in Appendix A.

Dependence on Scattering

L_{eff} is plotted as a function of the scattering coefficient in Figures 4.1 and 4.2. As can be seen in these figures, L_{eff} is less dependent on scattering for shorter vertical offsets. The magic distance would ideally yield a horizontal line in these plots (see Section 2.5.2). This is definitely not the case for long vertical offsets, but more similar to the curves for short offsets.

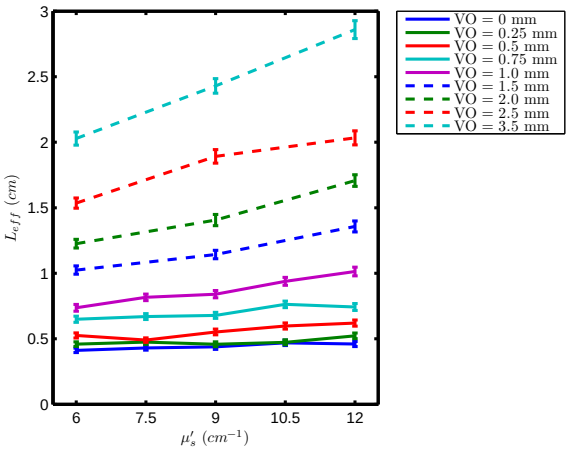

Figure 4.1: The effective path length (L_{eff}) with standard error as a function of scattering for $\mu_a = 0.5$ cm^{-1}.

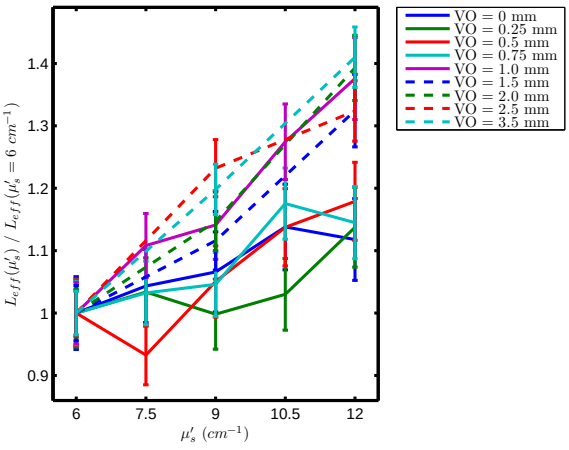

Figure 4.2: In this plot, L_{eff} is divided by L_{eff} at $\mu_s' = 6$ cm^{-1} for each vertical offset. All values are calculated for for $\mu_a = 0.5$ cm^{-1}.

Dependence on Vertical Offset

In Figures 4.3 and 4.4, L_{eff} is instead plotted as a function of vertical offset. As expected L_{eff} increases with vertical offset. L_{eff} is longer the higher the scattering, as it should be for vertical offsets longer than the magic distance (see Section 2.5.2). At the magic distance the lines should cross and change places. That they in principle do not, even for zero vertical offset, indicates that the magic distance is not reached probably due to the relatively large dimensions of the fibres. Still, the dependence on scattering is smaller for shorter vertical offsets.

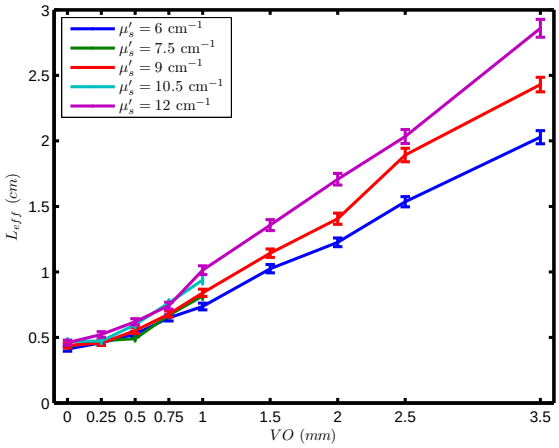

Figure 4.3: The effective path length (L_{eff}) with standard error as a function of vertical offset for $\mu_a = 0.5$ cm^{-1}.

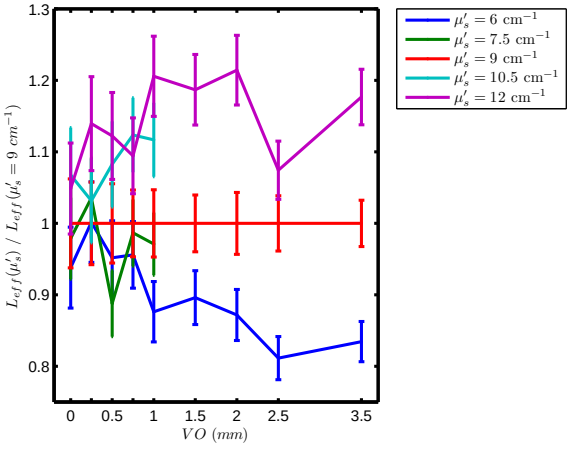

Figure 4.4: Here L_{eff} is divided by L_{eff} at $\mu_s' = 9$ cm^{-1} for each vertical offset. The absorption added after the simulations is $\mu_a = 0.5$ cm^{-1}.

Dependence on Absorption

Absorption is not included in the simulations, instead it is added afterwards in a procedure similar to white Monte Carlo (see Section 2.6.5). Thus L_{eff} can easily be plotted as a function of absorption coefficient, which is done in Figure 4.5 (a). L_{eff} decreases the higher the absorption, because the photons that travel longer are more affected by absorption.

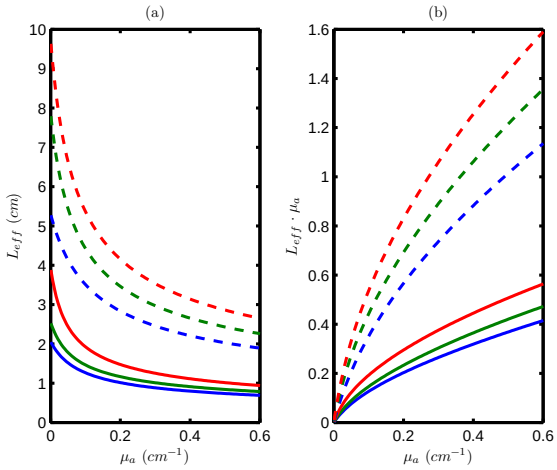

Figure 4.5: L_{eff} (a) and $L_{eff} \cdot \mu_a$ (b) as a function of μ_a. The solid lines are for $VO = 1$ mm whereas the broken lines are for $VO = 3.5$ mm. Blue, green and red show $\mu_s' = 6,\ 9$ and 12 cm^{-1}, respectively.

To be able to compare the simulation to the measurement, $L_{eff} \cdot \mu_a$ is plotted in Figure 4.5 (b). As μ_a is proportional to the concentration, c, according to equation 2.13, $L_{eff} \cdot \mu_a$ is proportional to $L_{eff} \cdot c$, which is the parameter plotted in Figure 4.9 for the measurements.

4.1.2 Simulated Flux

Although the main goal was to find the magic distance, one might want to compare to using the pivot point (as defined in Section 2.5.3). This is where the *detected flux* is least dependent on scattering. For that reason, the detected flux is plotted in Figures 4.6 and 4.7. At a first glance, they are very similar to Figures 4.1 and 4.2, but the order of the lines is reversed. Of course, a higher flux is detected the shorter the vertical offset. As opposed to the plots for L_{eff}, the detected flux is *less* dependent on scattering the longer the vertical offset. For very long vertical offsets, the detected flux should decrease with increased scattering. This vertical offset is not reached in the measurements, indicating that the pivot point is further away than 3.5 mm.

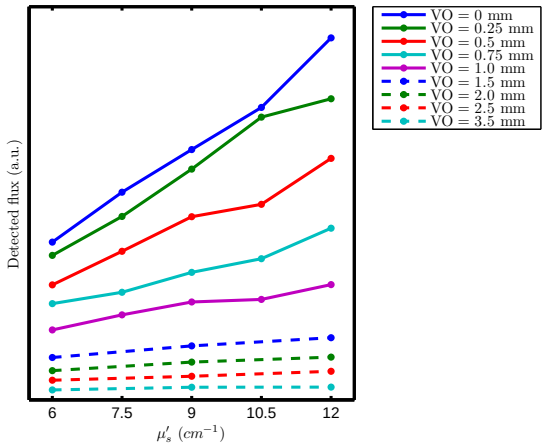

Figure 4.6: Detected flux as a function of scattering for $\mu_a = 0.5$ cm^{-1}.

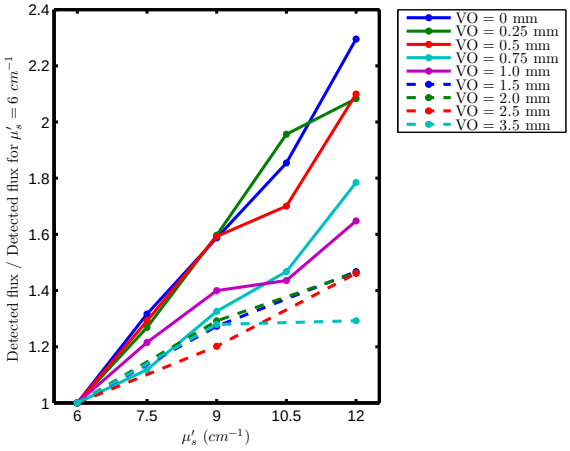

Figure 4.7: In this figure, L_{eff} is divided by L_{eff} at $\mu_s' = 6$ cm^{-1} for each vertical offset. The absorption coefficient used in these calculations is $\mu_a = 0.5$ cm^{-1}.

4.2 Measurements

Figure 4.8 shows example spectra measured for a phantom with $\mu_s' = 9$ cm^{-1} and $\mu_a = 0.5$ cm^{-1} and a vertical offset of 2 mm between the fibres. In (a) the spectra with (I) and without (I_0) the absorber (Methylene Blue) present in the tissue phantom can be seen. The absorbance according to equation 2.12 can be seen in (b), where also the result of the curve fitting is plotted. All curves are plotted in the interval 500-800 nm, the interval used for the evaluation. The absorption peak for Methylene Blue around 660 nm appears clearly and the fitted curve can be seen to follow the absorption spectrum closely.

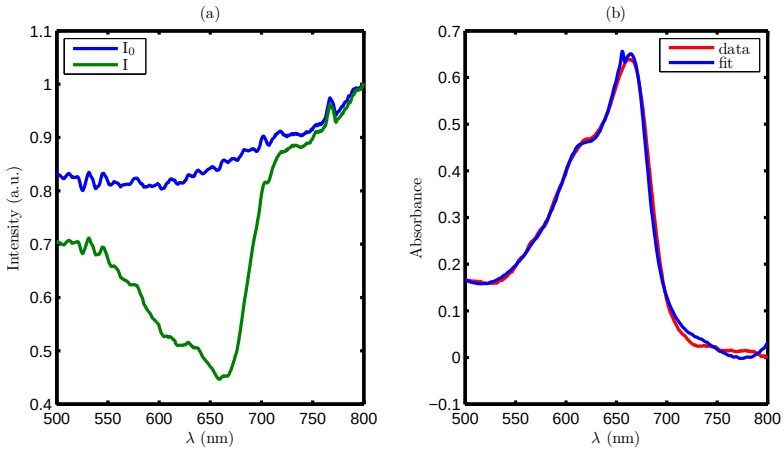

Figure 4.8: Example spectra for $\mu_s' = 9$ cm^{-1}, $\mu_a = 0.5$ cm^{-1} and VO = 2 mm showing the measured intensity (a) with (green) and without (blue) Methylene Blue present in the solution and the curve fitting (b) performed in Matlab showing both the measurement data (red) and the fitted curve (blue).

For each analysed spectrum the curve fitting algorithm returned values of $c \cdot L_{eff}$ for the absorbers included in the fitting procedure, in this case Methylene Blue, water and a set of free parameters. For our evaluation, only the Methylene Blue is interesting, thus these are the only results presented here. In Figure 4.9, some of the evaluated results are shown. The value of $c \cdot L_{eff}$ is plotted versus the absorption coefficient for the different scattering coefficients and different vertical offsets between the fibres, showing how the evaluated concentration for a given absorption varies with the scattering. This variation increases with the vertical distance between the fibre tips. These plots could also be compared to the simulation results in Figure 4.5. The shape of the curves is similar, although the order of the curves for the two highest scatterings is different. The reason for this is still to be found out.

4.2.1 Evaluation of the Optimal Fibre Separation

To evaluate the optimal distance between the fibre tips, i.e. the vertical offset, for which the measured absorption is insensitive to scattering, the variation in

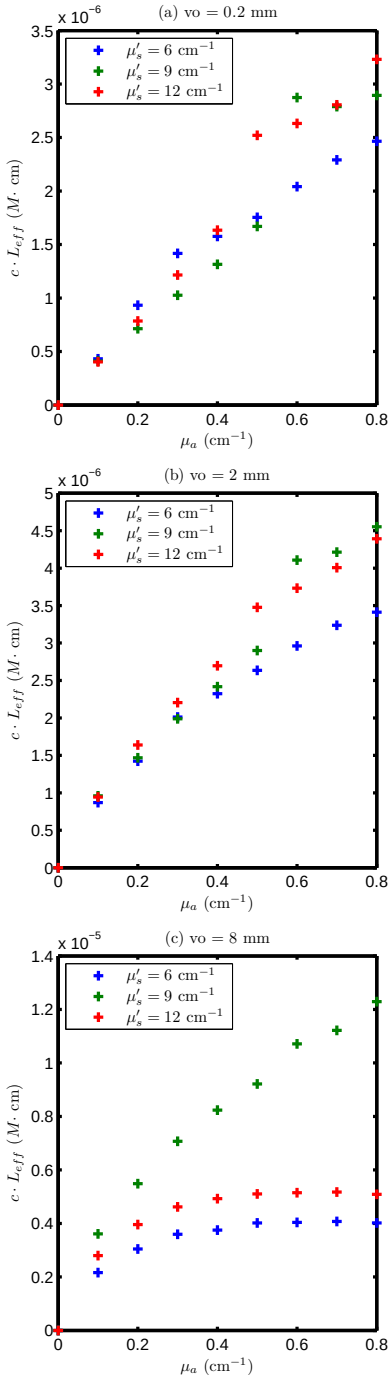

Figure 4.9: The evaluated value of $c \cdot L_{eff}$ plotted versus the absorption coefficient for VO = 0.2 mm, 2 mm and 8 mm.

the evaluated value of $c \cdot L_{eff}$, henceforth referred to as D, was investigated. For every vertical offset and every absorption, a mean value of D for the three different scattering coefficients was calculated, D_{mean}. The percent variation of D was then calculated according to Equation 4.1 for the set of different scattering coefficients.

$$percent\ variation = \delta_i = \frac{|D_i - D_{mean}|}{D_{mean}} \cdot 100 \tag{4.1}$$

Here, the index $i = 6, 9, 12$ denotes the scattering coefficient. For each value of the absorption coefficient, δ_i was calculated for every vertical offset. The results for the different scattering levels are seen in Figure 4.10. However, to be able to make an estimation of the optimal vertical offset, we need to identify the distance with the smallest maximal variation. Therefore, a plot showing the maximal percent variation compared to the mean value is presented in Figure 4.11. For each combination of absorption coefficient and vertical offset the highest value among δ_6, δ_9 and δ_{12} was plotted.

4.2.2 Error Evaluation

During the measurements we also studied the stability of the instrument and the phantom to be able to identify possible sources of error. Two different effects were observed. Fluctuations in the lamp intensity caused large variations in the measured intensity, which was seen to vary with 20 %. The signal strength was also affected by the temperature of the Intralipid phantom. A comparison between a phantom at room temperature and a phantom that had just been taken out of the refrigerator showed that a lower temperature of the phantom gave a higher signal.

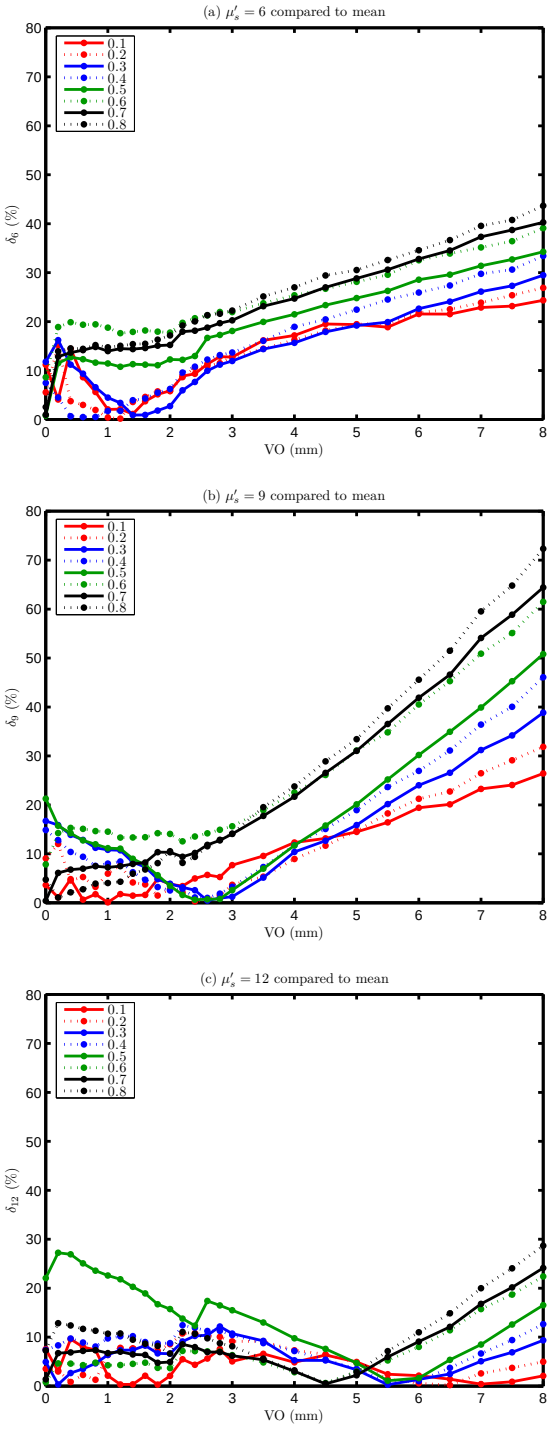

Figure 4.10: The percent variation in the evaluated value of D between the mean value and the result for the phantom with scattering coefficient $\mu_s' = 6$ cm^{-1}, $\mu_s' = 9$ cm^{-1} and $\mu_s' = 12$ cm^{-1}. The different curves denote the results for different absorption coefficients, as listed in the legend.

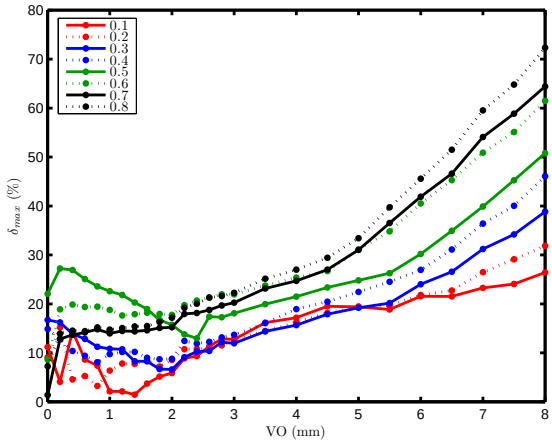

Figure 4.11: The maximum percent variation for the different values of the scattering coefficient in the evaluated value of D compared to the mean value for different vertical offsets. The different curves denote the results for different absorption coefficients, as listed in the legend.

Chapter 5

Discussion

The goal of the project was to measure absorption independent of scattering. To do this we wanted to find the vertical offset between the source fibre and the detection fibre where the effective photon path length, L_{eff}, varied the least with the scattering. This vertical offset has been referred to as the magic distance.

According to our simulations, L_{eff} varies less the shorter the vertical offset, indicating an optimal vertical distance shorter than 1 mm. This can be seen in Figures 4.1 to 4.4. Even at zero vertical offset, the photon paths are longer the higher the scattering, which according to the theory is true for fibre separations larger than the magic distance. This suggests that the magic distance is never reached. However, it does not mean that we would find the magic distance at negative vertical offsets, just that the fibre dimensions are too large.

The results from the measurements also imply that larger offsets cause larger variations in the absorption signal. In Figure 4.9 it can be seen that the value of the evaluated concentration varies more for larger than for smaller vertical offsets. From studying Figure 4.11, it is clear that this variation increases for vertical offsets larger than 2 mm, while it is more difficult to say something about the behaviour for smaller vertical offsets. An explanation for this might be that the fibre probe is less sensitive to absorption the smaller the offset between the fibres, since photons that have travelled a shorter distance are less likely to be absorbed.

Thus, there is a trade off between the low sensitivity to scattering at shorter offsets and the higher sensitivity to absorption at larger offsets. This suggests approximately 2 mm as the optimal vertical offset for concentration measurements for this probe and the tissue parameters used in this project. This is the same distance as that suggested by Mourant *et al.*[2,3] for a surface probe where the fibres are separated from each other instead of like in our case, where the tip of the detection fibre is pulled back from the tip of the source fibre.

5.1 The Magic Distance vs. the Pivot Point

In our work, we have focused on a probe design based on the magic distance, where L_{eff} varies the least with scattering. Another approach would have been to use the pivot point (as explained in Section 2.5.3), where the *detected intensity* varies the least with scattering. Our simulations indicates that this pivot point is further away than 3.5 mm, as can be seen in Figures 4.6 and 4.7. This can be compared to the pivot point for surface measurements where the fibres are separated from each other instead of pulled back, which is at approximately 3 mm in tissue according to Dam *et al.*[15] The difference in optimal fibre separation can be explained by the geometrical difference between interstitial and surface measurements.

An advantage with this approach would be that the probe would be more sensitive to absorption due to the longer distance between the fibres. On the other hand the longer distance also leads to a weaker detected signal.

5.2 Probe Design

The design suggested for the probe in this thesis is to use two thin optical fibres inside a brachytherapy needle. The probe is least sensitive to differences in scattering properties when the vertical offset between the source and detection fibre is 2 mm. Then concentrations could be measured with an accuracy of approximately 20 % in a simplified tissue phantom (see Figure 4.11).

5.3 Error Evaluation

For both simulations and measurements, the results rely on our choice of model and optical parameters. Both models are based on optical properties measured *in vivo*, but an important discrepancy is that while our models are homogeneous, real tissue is not. The intrinsic tissue parameters vary substantially within, as well as between, patients.[20]

In the simulations, other simulation parameters, like for instance when photons are terminated, affect the result. They are adjusted to influence the result as little as possible, while keeping the simulation times reasonable. Since Monte Carlo simulation is a statistical sampling, the accuracy of the result is strongly dependent on the number of rays traced. The expected magnitude of these errors are, however, easier to calculate statistically. These standard errors are the error bars shown in the plots. The requirement to detect at least 850 rays for each simulated geometry, seemed to yield sufficiently small error bars.

In the measurements, the results were influenced by substantial fluctuations in the lamp intensity. The offset was accounted for in the data evaluation, but we could not compensate for differences in the shape of the spectrum. The offset was seen to vary at least 20 %, while it is difficult to estimate the variations in shape,

which was often manifested as a varying slope of the spectrum over wavelength. The signal was also affected by the temperature of the phantom. This effect was minimized by always keeping the phantoms at room temperature during the measurements. Fluorescence of the Intralipid and the Methylene Blue could influence the results, but our data evaluation indicates that the fluorescence is limited. Another possible source of error is the accuracy of the mixing of the phantoms. This error could be assessed with repeated measurements, which has not been done due to the limited time frame of this project.

5.4 Outlook

To improve the reliability of the measurements, the next step would be to estimate the uncertainties by repeating the experiments. As the final goal would be a clinically applicable device, the natural continuation is to evaluate the probe under increasingly realistic conditions. This would include phantoms containing background absorption and a real photochemical substance, measurements in meat and finally *in vivo* trials. It would also be interesting to compare the present probe to alternative designs, for instance surface probes. This could be done both through measurements and simulations.

Chapter 6

Conclusions

In this project we have arrived at a probe design for interstitial concentration measurements. To be able to measure interstitially, the source and detection fibres are fitted inside a needle. The detection fibre is pulled back a certain distance in order to measure absorption independent of scattering. Through simulations the probe was found to be less sensitive to scattering the shorter this distance. This is not contradicted by the measurements, which support a vertical offset of 2 mm or shorter. On the other hand the sensitivity to absorption increases the larger the offset. Consequently, we suggest a vertical offset of 2 mm between the source fibre and the detection fibre in the probe.

Chapter 7

Acknowledgements

First of all, we would like to thank our supervisors Stefan Andersson-Engels and Ann Johansson for making this thesis possible and for giving us the opportunity to join the medical laser physics group for a while. We appreciate the inspiring discussions and helpful comments on our work. Special thanks to Ann for always answering our questions, helping us with evaluating the results and reading the manuscript. We would also like to thank Tomas Svensson for helping us with our deep concern regarding the standard error calculations and for taking masterly photos of our setup. Additionally, we would like to thank the rest of the group, Johan Axelsson and Jenny Svensson, for being helpful and welcoming.

When we struggled to learn ASAP* ASAP†, Linda Persson, Elias Kristensson and Mats Andersson provided valuable help. We are also grateful to Bertil Hermansson for helping out with computers and software and to Tomas Remetter for assisting us in our experimenting with metal coating of the fibres.

We would also like to thank our fellow diploma students at the division for their nice company, especially our room mates Johan Tholén and Tran Thi Thu Tam for many long and interesting discussions.

Last, but not least, we would like to thank NIH for the funding through the NTROI project coordinated by Irving Bigio at Boston University.

*Advanced Systems Analysis Program
†As Soon As Possible

Bibliography

[1] M. Soto Thompson. *Photodynamic Therapy Utilizing Interstitial Light Delivery Combined with Spectroscopic Methods.* Doctoral thesis, Lund Institute of Technology, Lund, 2004.

[2] J.R. Mourant, T.M. Johnson, G. Los, and I.J. Bigio. Non-invasive measurement of chemoterapy drug concentrations in tissue: Preliminary demonstrations of in vivo measurements. *Physics in Medicine and Biology*, 44:1397–1417, 1999.

[3] J.R. Mourant, I.J. Bigio, D.A. Jack, T.M. Johnson, and H.D. Miller. Measuring absorption coefficients in small volumes of highly scattering media: Source-detector separations for which path lengths do not depend on scattering properties. *Applied Optics*, 36(22):5655–5661, 1997.

[4] J. Swartling. *Biomedical and Atmospheric Applications of Optical Spectroscopy in Scattering Media.* Doctoral thesis, Lund Institute of Technology, Lund, 2002.

[5] A.J. Welch and M.J.C. van Gemert. *Optical-Thermal Response of Laser-Irradiated Tissue*, chapter 2. Plenum Press, New York, 1995.

[6] C. Abrahamsson. *Time-Resolved Spectroscopy for Pharmaceutical Applications.* Doctoral thesis, Lund Institute of Technology, Lund, 2005.

[7] J.-L. Boulnois. Photophysical processes in recent medical laser developments: a review. *Lasers in Medical Science*, 1:47–66, 1986.

[8] F.L. Pedrotti and L.S. Pedrotti. *Introduction to Optics.* Prentice Hall, New Jersey, 2nd edition, 1993.

[9] S. Svanberg. *Atomic and Molecular Spectroscopy - Basic Aspects and Practical Applications.* Springer Verlag, 4th edition, 2004.

[10] C. af Klinteberg. *On the Use of Light for the Characterization and Treatment of Malignant Tumours.* Doctoral thesis, Lund Institute of Technology, Lund, 1999.

[11] A.J. Welch and M.J.C. van Gemert. *Optical-Thermal Response of Laser-Irradiated Tissue*, chapter 9. Plenum Press, New York, 1995.

[12] Fluorescence imaging with medical applications. http://kurslab.fysik.lth.se/Multi/FI-2006.pdf. Laboration manual, multispectral imaging (Division of Atomic Physics, LTH), accessed 12.12.2006.

[13] Sven-Göran Pettersson, Stefan Andersson-Engels, and Stefan Kröll. *Photonics and Optical Communication*, chapter Fibre Optics. Lund, 2005.

[14] C. Eker. *Optical Characterization of Tissue for Medical Diagnostics*. Doctoral thesis, Lund Institute of Technology, Lund, October 1999.

[15] J.S. Dam. *Optical Analysis of Biological Media - Continuous Wave Diffuse Spectroscopy*. Doctoral thesis, Lund Institute of Technology, Lund, November 2000.

[16] I.J. Bigio and J.R. Mourant. Ultraviolet and visible spectroscopies for tissue diagnostics: Fluorescence spectroscopy and elastic-scattering spectroscopy. *Physics in Medicine and Biology*, 42(5):803–814, May 1997.

[17] A. Sharwani, W. Jerjes, V. Salih, B. Swinson, I.J. Bigio, M. El-Maaytah, and C. Hopper. Assessment of oral premalignancy using elastic scattering spectroscopy. *Oral Oncology*, 42(4):343–349, April 2006.

[18] A. Dhar, K.S. Johnson, M.R. Novelli, S.G. Bown, I.J. Bigio, L.B. Lovat, and S.L. Bloom. Elastic scattering spectroscopy for the diagnosis of colonic lesions: initial results of a novel optical biopsy technique. *Gastrointestinal Endoscopy*, 63(2):257–261, February 2006. 2006.

[19] S.A. Prahl, M. Keijzer, S.L. Jaques, and A.J. Welch. A monte carlo model of light propagation in tissue. *SPIE Institute Series*, IS 5, 1989.

[20] Tomas Svensson, Stefan Andersson-Engels, Margrét Einarsdóttír, and Katarina Svanberg. In vivo optical characterization of human prostate tissue using near-infrared time-resolved spectroscopy. *Journal of Biomedical Optics*, 12(1):014022, 2007.

[21] Inc. Breault Research Organization. *The ASAP^{TM} Primer*. Tucson, 2005.

[22] Inc. Breault Research Organization. Using voxels in asap^{TM} modeling fluorescence and volume scatter. *ASAP Procedural Note*, 2005.

[23] S. A. Prahl. Tabulated molar extinction coefficient for methylene blue in water. http://omlc.ogi.edu/spectra/mb/mb-water.html. Accessed 10.01.2007.

Appendix A

Calculation of the Effective Path Length

A.1 The Effective Path Length (L_{eff})

This appendix describes how the effective path length L_{eff} (as defined on page 14) and its standard error were calculated from the simulated path lengths. The effective path length is the path length that can replace the full path length distribution in the Beer Lambert law. Because of the exponential dependence it is not equal to the average path length $\langle L \rangle$.

$$I = I_0\, e^{-\mu_a L_{eff}} \quad \Rightarrow \quad L_{eff} = \frac{ln\left(\frac{I_0}{I}\right)}{\mu_a} \tag{A.1}$$

To calculate L_{eff} from the simulated path lengths, I and I_0 have to be calculated. I is the total detected intensity, i.e. the sum of the fluxes ϕ_i of the n individual rays. Each ϕ_i can be calculated from the flux when the ray starts out, ϕ_0, and its path length, L_i, through the Beer Lambert law:

$$I = \sum_{i=1}^{n} \phi_i = \sum_{i=1}^{n} \left(\phi_0\, e^{-\mu_a L_i}\right) = \phi_0 \sum_{i=1}^{n} e^{-\mu_a L_i} \tag{A.2}$$

I_0 is the detected intensity if there would be no absorption, i.e. the sum of the original fluxes of all the rays that eventually reach the detector:

$$I_0 = \sum_{i=1}^{n} \phi_i(\mu_a = 0) = \sum_{i=1}^{n} \left(\phi_0\, e^{-0 \cdot L_i}\right) = \sum_{i=1}^{n} \phi_0 = n \cdot \phi_0 \tag{A.3}$$

When all this is put together, L_{eff} can be calculated from the simulated path lengths, L_i:

$$L_{eff} = \frac{ln\left(\frac{I_0}{I}\right)}{\mu_a} = \frac{ln\left(\frac{n \cdot \phi_0}{\phi_0 \sum_{i=1}^{n} e^{-\mu_a L_i}}\right)}{\mu_a} = \frac{ln\left(\frac{n}{\sum_{i=1}^{n} e^{-\mu_a L_i}}\right)}{\mu_a} = -\frac{ln\left\langle e^{-\mu_a L_i}\right\rangle}{\mu_a} \tag{A.4}$$

A.2 The Standard Error ($\sigma_{L_{eff}}$)

The standard error was calculated to estimate the uncertainty of the simulated L_{eff}. To simplify the calculations, x_i was defined as

$$x_i \equiv e^{-\mu_a L_i} \tag{A.5}$$

with the average

$$\bar{x} = \frac{1}{n}\sum_{i=1}^{n} x_i \tag{A.6}$$

and standard deviation

$$s_x = \sqrt{\frac{1}{n-1}\sum_{i=1}^{n}\left(x_i - \bar{x}\right)^2} \ . \tag{A.7}$$

The standard deviation of the mean $\bar{x}$, or its standard error, is then

$$\sigma_{\bar{x}} = \frac{s_x}{\sqrt{n}} \ . \tag{A.8}$$

With these definitions, the formula for L_{eff} simplifies to

$$L_{eff} = -\frac{ln\left(\bar{x}\right)}{\mu_a} \tag{A.9}$$

and its standard error becomes

$$\sigma_{L_{eff}} = \left|\frac{\partial L_{eff}}{\partial \bar{x}}\right| \sigma_{\bar{x}} = \left|-\frac{1}{\mu_a \bar{x}}\right| \sigma_{\bar{x}} = \frac{\sigma_{\bar{x}}}{\mu_a \bar{x}} \ . \tag{A.10}$$

Appendix B

ASAP Example Code

```
!! Simulation where VO and MUS are varied and MUA=0.

!! Constants
VO=0          !! Vertical Offset (pullback) (cm)
HO=0.0401     !! Horizontal Offset, center to center distance (cm)
EFO=1E-7      !! Emission Fiber vertical Offset (cm)
TSR=2.5       !! Tissue Sphere Radius (cm)

ECO=0.0300    !! Emitter COre diameter (cm)
ECL=0.0330    !! Emitter CLadding diameter (cm)
EJ=0.0400     !! Emitter Jacket diameter (cm)
EL=6          !! Emitter Length (cm)

DCO=0.0300    !! Detector COre diameter (cm)
DCL=0.0330    !! Detector CLadding diameter (cm)
DJ=0.0400     !! Detector Jacket diameter (cm)
DL=6          !! Detector Length (cm)

G=0.85        !! g for tissue
MUS=60        !! mus (not mus') for tissue
MUA=0         !! mua for tissue

NR=1E6        !! Number of Rays
EHA=9.04      !! Emission Half Angle (degrees)

$DO 100 10000 1
{

!! Name of the result files: pswa[C=run number][B*0.05=VO][A*10=MUS].type

A=?\10
B=[(?\100)-A]/10
```

```
MUS=A*10
VO=B*0.05

$IF (MUS) EQ 40 OR (MUS) EQ 60 OR (MUS) EQ 80 AND (VO) LT 0.3 THEN

!! Reset system
$TIC
SYSTEM NEW
RESET
SEED

!! System settings
UNITS CENTIMETERS 'W'
WAVELENGTH 660 NM
LEVEL 1E7
HALT 1E3 1E-6
CUTOFF 1E-18 1E3

!! Coating definitions
COATING PROPERTIES
  0 0 'ABSORB'
  0 1 'TRANSMIT'
  1 0 'REFLECT'
  0.99 0 'ALUMINIUM'

!! Media definitions
MODELS
  VOLUME (G) (MUS)‘(MUA) 1  !! g, mus, mua, obscuration=1

MEDIA
  1.4 SCATTER 1 0 1 1E7 1E7 'TISSUE'
  1.4 'SURROUNDINGS'
  1.457 'CORE'
  1.440 'CLADDING'
  0.0292‘3.92 ABSORB 'ALUMINIUM' !! n at 550 nm from exercise in Pedrotti

!! Reflection settings
FRESNEL AVE
SPLIT 1 MONTECARLO

!! Detector (1)
SURFACE
  PLANE Y (VO) ELLIPSE DCO/2 DCO/2 0
  SHIFT X (HO)
OBJECT 'DETECTOR'
  INTERFACE COATING ABSORB TISSUE CORE
  REDEFINE COLOR 3

!! Emission fiber core (2-4)
SURFACE
```

```
  PLANE Y (EFO) ELLIPSE ECO/2 ECO/2 0 0
OBJECT 'EF.CORE.TIP'
  INTERFACE COATING BARE CORE TISSUE
  REDEFINE COLOR 1

SURFACE
  TUBE Y (EFO) ECO/2 ECO/2 EFO+EL ECO/2 ECO/2
OBJECT 'EF.CORE.SIDE'
  INTERFACE COATING BARE CORE CLADDING
  REDEFINE COLOR 1

SURFACE
  PLANE Y EFO+EL ELLIPSE ECO/2 ECO/2 0 0
OBJECT 'EF.CORE.TOP'
  INTERFACE COATING ABSORB CORE SURROUNDINGS
  REDEFINE COLOR 1

!! Emission fiber cladding (5-7)
SURFACE
  PLANE Y (EFO) ELLIPSE ECL/2 ECL/2 ECO/ECL 0
OBJECT 'EF.CLADDING.TIP'
  INTERFACE COATING BARE CLADDING TISSUE
  REDEFINE COLOR 22

SURFACE
  TUBE Y (EFO) ECL/2 ECL/2 EFO+EL ECL/2 ECL/2
OBJECT 'EF.CLADDING.SIDE'
  INTERFACE COATING BARE CLADDING ALUMINIUM
  REDEFINE COLOR 22

SURFACE
  PLANE Y EFO+EL ELLIPSE ECL/2 ECL/2 ECO/ECL 0
OBJECT 'EF.CLADDING.TOP'
  INTERFACE COATING ABSORB CLADDING SURROUNDINGS
  REDEFINE COLOR 22

!! Emission fiber jacket (8-10)
SURFACE
  PLANE Y (EFO) ELLIPSE EJ/2 EJ/2 ECL/EJ 0
OBJECT 'EF.JACKET.TIP'
  INTERFACE COATING BARE ALUMINIUM TISSUE
  REDEFINE COLOR 20

SURFACE
  TUBE Y (EFO) EJ/2 EJ/2 EFO+EL EJ/2 EJ/2
OBJECT 'EF.JACKET.SIDE'
  INTERFACE COATING BARE ALUMINIUM TISSUE
  REDEFINE COLOR 20

SURFACE
```

```
  PLANE Y EFO+EL ELLIPSE EJ/2 EJ/2 ECL/EJ 0
OBJECT 'EF.JACKET.TOP'
  INTERFACE COATING ABSORB ALUMINIUM SURROUNDINGS
  REDEFINE COLOR 20

!! Detection fiber core (-detector) (11-12)
SURFACE
  TUBE Y (VO) DCO/2 DCO/2 VO+DL DCO/2 DCO/2
  SHIFT X (HO)
OBJECT 'DF.CORE.SIDE'
  INTERFACE COATING BARE CORE CLADDING
  REDEFINE COLOR 1

SURFACE
  PLANE Y VO+DL ELLIPSE DCO/2 DCO/2 0 0
  SHIFT X (HO)
OBJECT 'DF.CORE.TOP'
  INTERFACE COATING ABSORB CORE SURROUNDINGS
  REDEFINE COLOR 1

!! Detection fiber cladding (13-15)
SURFACE
  PLANE Y (VO) ELLIPSE DCL/2 DCL/2 DCO/DCL 0
  SHIFT X (HO)
OBJECT 'DF.CLADDING.TIP'
  INTERFACE COATING BARE CLADDING TISSUE
  REDEFINE COLOR 22

SURFACE
  TUBE Y (VO) DCL/2 DCL/2 VO+DL DCL/2 DCL/2
  SHIFT X (HO)
OBJECT 'DF.CLADDING.SIDE'
  INTERFACE COATING BARE CLADDING ALUMINIUM
  REDEFINE COLOR 22

SURFACE
  PLANE Y VO+DL ELLIPSE DCL/2 DCL/2 DCO/DCL 0
  SHIFT X (HO)
OBJECT 'DF.CLADDING.TOP'
  INTERFACE COATING ABSORB CLADDING SURROUNDINGS
  REDEFINE COLOR 22

!! Detection fiber jacket (16-18)
SURFACE
  PLANE Y (VO) ELLIPSE DJ/2 DJ/2 DCL/DJ 0
  SHIFT X (HO)
OBJECT 'DF.JACKET.TIP'
  INTERFACE COATING BARE ALUMINIUM TISSUE
  REDEFINE COLOR 20
```

```
SURFACE
  TUBE Y (VO) DJ/2 DJ/2 VO+DL DJ/2 DJ/2
  SHIFT X (HO)
OBJECT 'DF.JACKET.SIDE'
  INTERFACE COATING BARE ALUMINIUM TISSUE
  REDEFINE COLOR 20

SURFACE
  PLANE Y VO+DL ELLIPSE DJ/2 DJ/2 DCL/DJ 0
  SHIFT X (HO)
OBJECT 'DF.JACKET.TOP'
  INTERFACE COATING ABSORB ALUMINIUM SURROUNDINGS
  REDEFINE COLOR 20

!! Prostate (19)
SURFACE
  ELLIPSOID (TSR) (TSR) (TSR)
OBJECT 'PROSTATE'
  INTERFACE COATING TRANSMIT TISSUE SURROUNDINGS
  BOUNDS 9 17
  REDEFINE COLOR 14

!! Source definitions
IMMERSE TISSUE
EMITTING DISK -Y 0 ECO/2 ECO/2 (NR) (EHA) (EHA)
FLUX TOTAL 1

!! Ray tracing
SAVE 10
!!WINDOW X Y
!!PLOT FACETS 5 5 OVERLAY
!!MISSED ARROWS 1.0
!!TRACE PLOT
!!$VIEW
$IO OUTPUT PSWA?.TRA BOTH
TRACE
$TIC
STATS
$IO OUTPUT CLOSE

!! Analysis
CONSIDER ONLY DETECTOR
SELECT ONLY .98758 B

$IO OUTPUT PSWA?.POS ONLY
LIST POSITION
$IO OUTPUT CLOSE

$IO OUTPUT PSWA?.DIR ONLY
LIST DIRECTION
```

```
$IO OUTPUT CLOSE

$IO OUTPUT PSWA?.HIS ONLY
HISTORY 10
$IO OUTPUT CLOSE

$GUI RemoteSendFile . "PSWA?.*"

CONSIDER ALL
SELECT ALL
RETURN

$ENDIF
}
```